A Status Report
Grant No. NAG 5-865
January 1, 1987 - May 31, 1987

MICROGRAVITY NUCLEATION AND PARTICLE COAGULATION EXPERIMENTS SUPPORT

Submitted to:

National Aeronautics and Space Administration
Goddard Space Flight Center
Greenbelt, Maryland 20771

Attention: Dr. Joseph A. Nuth, III
Code 691

Submitted by:

L. U. Lilleleht
Associate Professor

T. J. Lass
Graduate Assistant

Report No. UVA/528260/CHE88/101
December 1987

SCHOOL OF ENGINEERING AND APPLIED SCIENCE

DEPARTMENT OF CHEMICAL ENGINEERING

UNIVERSITY OF VIRGINIA
CHARLOTTESVILLE, VIRGINIA 22901

MICROGRAVITY NUCLEATION AND PARTICLE COAGULATION EXPERIMENTS SUPPORT

Status Report I

For the Period January-May 1987

Submitted To

National Aeronautics and Space Administration
Goddard Space Flight Center
Greenbelt, Maryland 20771

For Work Performed under Grant NAG 5-865
by
Lembit U. Lilleleht and Timothy J. Lass

Department of Chemical Engineering
School of Engineering and Applied Science
University of Virginia
Charlottesville, Virginia 22901

Report No. UVA/528260/CHE88/101

Copy No. _____

December 1987

ABSTRACT

This report summarizes the work performed at the University of Virginia on "Microgravity Nucleation and Particle Coagulation Experiments Support," under a grant NAG 5-865 covering the time period through May 1987.

A hollow sphere model is developed to predict the range of supersaturation ratio values for refractory metal vapors in a proposed experimental nucleation apparatus. Since the experiments are to be carried out in a microgravity environment, the model neglects the effects of convection and assumes that the only transfer of vapors through a inert gas atmosphere is by conduction and molecular diffusion.

A consistent set of physical properties data is assembled for the various candidate metals and inert ambient gases expected to be used in the nucleation experiments.

Transient partial pressure profiles are computed for the diffusing refractory species for two possible temperature distributions. The supersaturation ratio values from both candidate temperature profiles are compared with previously obtained experimental data on a silver-hydrogen system.

The model is used to simulate the diffusion of magnesium vapor through argon and other inert gas atmospheres over ranges of initial and boundary conditions. These results identify different combinations of design and operating parameters which are likely to produce supersaturation ratio values high enough to induce homogeneous nucleation in the apparatus being designed for the microgravity nucleation experiments.

Table of Contents

List of Figures

List of Tables

Chapter 1
INTRODUCTION

In the last twenty years, many scientists have become interested in the homogeneous nucleation of refractory materials such as metals and their oxides and carbon and its compounds. NASA is particularly interested in this subject because these materials are found throughout the interstellar medium, and NASA wants to determine their origin. Are they products of condensation of released vapors from stars? Or is there some other explanation? One possibility is that these particles were formed from very hot vapors in stellar outflows and as these vapors cooled, they condensed and grew into larger particles.

A comprehensive program to study the nucleation of refractory materials is being undertaken to gain a better understanding of how particles nucleate and grow in the environment of outer space. Some experiments have already been performed in various terrestrial laboratories to determine the nucleation characteristics of individual substances, including the Goddard Space Flight Center studies of the vapor phase condensation of SiO and Ag [1,2]. In order to minimize the possible effect of convection arising from the temperature gradients in the gravitational field, a series of experiments is now being designed to extend this work to a microgravity environment.

In this chapter, the Classical Homogeneous Nucleation Theory and Rasmussen's adjustment to the Classical Theory will be reviewed. These

theories will then be applied to the condensation data of SiO and Ag. Finally, a preview of my thesis will be discussed.

1.1. Classical Homogeneous Nucleation Theory

The concept of homogeneous nucleation, first discussed by J. Willard Gibbs and subsequently developed into the Classical Homogeneous Nucleation Theory by Becker and Doring [3,4], is based on the premise that there is a barrier to the nucleation of a condensed phase from the vapor phase. This barrier is associated with the energy required to create a new surface and can be expressed in terms of the Gibbs free energy, ΔG, given by the following equation:

$$\Delta G = -nkT\ln(S) + A\gamma \tag{1.1}$$

where the first term is the energy released by the transfer of n moles from the vapor phase to a cluster of the condensed phase, and the second term accounts for the interfacial surface energy of the cluster. S is the supersaturation ratio, k is the Boltzmann constant, A is the surface area of the cluster and γ is the interfacial tension of the cluster at the temperature T.

The embryo, which is a cluster of atoms or molecules from the vapor phase, either grows or decays when another monomer collides with the cluster. If the addition of a monomer increases the surface energy more than it gives up due to condensation, then ΔG increases and the embryo is destabilized thereby inhibiting the onset of nucleation. The embryo could

continue to grow, however, by the addition of monomers until the barrier to nucleation is overcome when the rate of increase in the surface tension effects equals the rate of decrease in the energy from condensation. At this point, the embryo has reached a critical size: ΔG has reached a maximum, and the addition of one more monomer would cause a decrease in ΔG and a nucleus has been formed. By a nucleus is meant a cluster of atoms or molecules for which the addition of an additional monomer first results in a decrease in ΔG.

Adamson [5] presents a system of equations from which the critical radius of the nucleus, the maximum Gibbs free energy and the nucleation rate can be calculated. First, a spherical geometry is assumed for the cluster and eqn.(1.1) becomes:

$$\Delta G = -\frac{4}{3}\pi r^3 \frac{kT}{V}\ln(S) + 4\pi r^2\gamma \tag{1.2}$$

where r is the radius of the cluster and V is the volume per molecule of the condensed phase.

The critical radius, r_c, is the minimum radius, beyond which the addition of another monomer reduces ΔG, and is obtained by locating the maximum in the ΔG vs. r curve (see Fig. 1-1). The critical radius can be found by differentiating eqn.(1.2) with respect to r and setting the derivative equal to zero. Then solving the resulting equation for r, gives the critical radius needed to maximize the Gibbs free energy:

$$r_c = \frac{2\gamma V}{kT\ln(S)} \tag{1.3}$$

Now, the maximum Gibbs free energy, ΔG_{max}, is obtained by substituting eqn.(1.3) into eqn.(1.2):

$$\Delta G_{max} = \frac{16\pi\gamma^3 V^2}{3(kT\ln(S))^2} \tag{1.4}$$

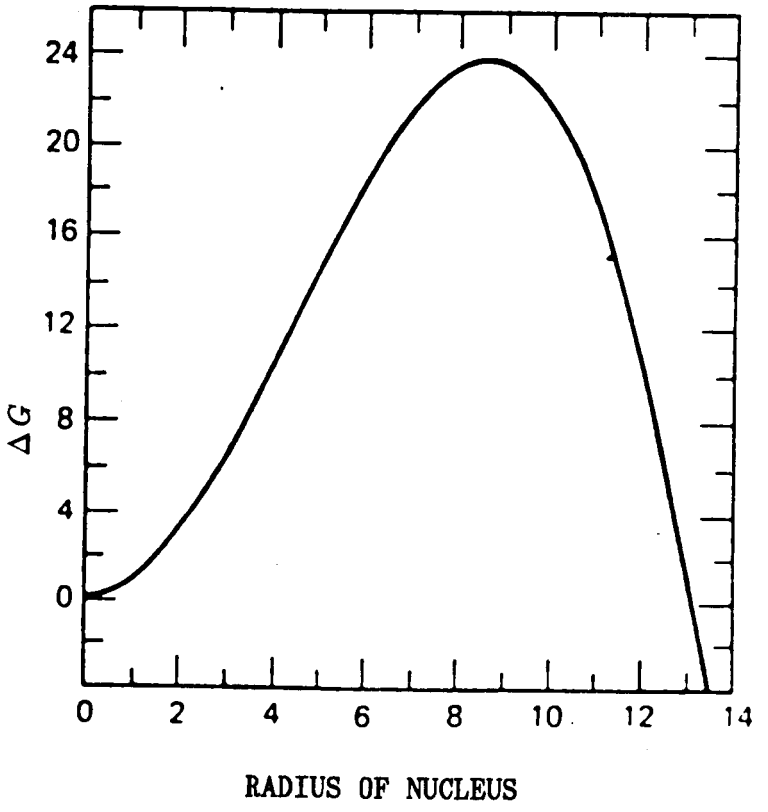

Figure 1-1: Gibbs free energy vs. Radius of nucleus [5]

The nucleation rate, J, is related to ΔG_{max} and the rate of formation of clusters of atoms or molecules. Since J is assumed to be the same for any size nucleus, it will be proportional to the gas kinetic collision frequency, Z. The consequence of this is that J equals the rate of formation of a cluster of two atoms or molecules modified by an activation energy term. This yields the following approximate relationship:

$$J = Z\exp(\frac{-\Delta G_{max}}{kT}) \tag{1.5}$$

A more complete expression of the nucleation rate according to the Becker-Doring development is given by the following equation:

$$J = \frac{\sqrt{2\gamma}}{\sqrt{\pi m}} V N_1^{\,2} exp(\frac{-16\pi\gamma^3 V^2}{3(kT)^3(\ln(S))^2}) \tag{1.6}$$

where N_1 is the concentration of a single monomer and m is the mass of a condensing monomer [6].

Two assumptions of the Classical Theory have come under attack in recent years. The first assumption being questioned is the capillarity approximation which assumes that the properties of a small cluster are the same as those of the condensed bulk phase. The second questionable assumption is the existence of a state of local thermodynamic equilibrium around the nucleation site. The questioning of these two assumptions have led to reanalyses of the Classical Theory.

1.2. Rasmussen's Adjustment to the Classical Theory

Don H. Rasmussen's adjustment to the Classical Theory [7,8] is based partly on the work of Cahn and Hilliard [9] in which the idea of a physical spinodal had been developed. A physical spinodal is a thermodynamic limit to the metastability of a parent phase. It occurs at a critical supersaturation point and a critical cluster size such that, when this limit is reached, there is no longer any barrier to nucleation. The Classical Theory does not predict such a limit because the Classical Theory always assumes that there is a barrier to nucleation. To obtain a physical spinodal, Rasmussen assumed that a constant pressure exists throughout the supersaturated system. This assumption implies that the chemical potential is a continuous function of the cluster size which leads to the development of a physical spinodal. Constant pressure also implies that the surface tension of a nucleus is dependent on the size of the nucleus. This is similar to the earlier results by Cahn and Hilliard; and, therefore, Rasmussen was able to eliminate the capillarity approximation from the Classical Theory.

One way to test the Rasmussen Theory is by using the linear relationship between the temperature, T_n, at which nucleation occurs, and the temperature, T_{eq}, at which the system would be when at equilibrium, which is predicted by the Rasmussen Theory and is given by the following equation:

$$T_{eq} = K^{-1}T_n + T_c(1 - K^{-1}) \tag{1.7}$$

where T_c is the critical temperature for the system being studied. K is a

constant based on the temperature dependence of the surface tension, the difference in entropy between phases on the curve at the surface interface and the temperature dependence of interface thickness. K has a value of approximately 1.25 for organic vapor-liquid systems and inorganic liquid-liquid systems. However, there is no explanation as to why K should be the same for all these systems. K may be different for systems that involve refractory materials.

1.3. Analysis of Previous Experiments

Two experimental techniques have been used to study the nucleation of refractory materials. One technique incorporates the use of a shock tube and has been used primarily by Bauer et al. [10,11]. These experiments must be run at high pressure and temperature, and the nucleation rate must be of the order of magnitude of 10^{12} to 10^{18} $cm^{-3}sec^{-1}$. Basically, a shock wave dissociates the refractory material in a matter of microseconds and nucleation occurs during the gas expansion. There are several disadvantages to the shock tube technique. First, studies are limited to refractory materials that have volatile precursors. For example, Bi is introduced as $Bi(CH_3)_3$, Fe is introduced as $Fe(CO)_3$ and Pb is introduced as $Pb(CH_3)_4$. Second, the experiments occur on an extremely fast time scale (nucleation occurs in a few milliseconds). Third, the experiments are basically "one shot" in nature. That is, if nucleation does not occur in a matter of milliseconds, then nucleation will probably not occur at any later time, and the whole process must be repeated. Last, the temperature at the point of nucleation cannot be determined with a high degree of accuracy.

The second experimental technique involves a direct vaporization-

condensation process. The refractory material is heated in a crucible. Its vapor is released into an inert gas atmosphere where the material nucleates and a cloud of condensed material can be visually observed. Hence, this technique is often referred to as the cloud-chamber technique. An advantage of this technique is that the temperature profile can be controlled and therefore nucleation can be controlled by adjusting the supersaturation ratio. Disadvantages are due to the convective instabilities which may arise from the difference in temperature between the very hot source and the much cooler ambient atmosphere, and the difficulties related to melting and vaporization of refractory materials.

The Classical Theory has been applied to both techniques, but most of my study will involve the vaporization-condensation or cloud-chamber technique. Nuth et al. [1,2] attempted to use the Classical Theory and the Rasmussen Theory to analyze their results from the study of the condensation of SiO and Ag. These results indicated that neither the Classical Theory nor the Rasmussen Theory fit their refractory materials condensation data.

A primary assumption of the Classical Theory is the capillarity approximation which assumes that the properties of a small cluster are the same as for the condensed bulk phase. This approximation may have an effect on the expected nucleation rate due to the use of the bulk phase value of the surface tension. For very small clusters, there may be some effect of curvature on the surface tension which would mean that the surface tension of a small cluster is not the same as for the condensed bulk phase [5,12]. However, there are not enough data available to determine how much of an effect curvature has on the surface tension of very small clusters.

If the capillarity approximation is valid, then m, V and γ in eqn.(1.6) can be assigned their bulk phase values. Eqn.(1.6) can then be rearranged so that

$$\ln(N_1^2) = \frac{C_2\gamma^3}{T^3(\ln(S))^2} + \ln\left(\frac{J}{C_1\gamma^{0.5}}\right) \tag{1.8}$$

where

$$C_1 = \frac{\sqrt{2V^2}}{\sqrt{\pi m}}$$

$$C_2 = \frac{16\pi V^2}{3k^3}$$

If it is further assumed that the surface tension is constant over the range of temperatures covered by the given series of experiments, then, according to eqn.(1.8), a plot of $T^{-3}\ln(S)^{-2}$ vs. $\ln(N_1^2)$ should be linear. However, the results from a previous study of the condensation of Ag shows that a straight line is not obtained as would be expected from the Classical Theory [2]. The results from the study of the condensation of SiO does result in a straight line, but the calculated values for the critical radius and nucleus is unreasonable [1].

Another assumption of the Classical Nucleation Theory is that the molecular or atomic components are assumed to be in a state of local thermodynamic equilibrium (LTE). Computer modeling of the condensation of SiO by Nuth et al. [13] seems to contradict this assumption for

circumstellar environments. There is believed to be a significant degree of vibrational disequilibrium existing in the regions of circumstellar nucleation. This state of disequilibrium may aid the onset of nucleation in two ways. First, a larger proportion of SiO monomers will occupy lower vibrational levels under non-LTE conditions. The rate of formation of SiO dimers should then increase because the average SiO-SiO complex will have less energy than is expected for LTE conditions. Second, the rate at which the SiO dimers are dissociated due to collisions would decrease which means that there should be a large increase in the concentration of SiO dimers under non-LTE conditions. An increase in the concentration of SiO dimers should lead to an increased rate at which stable nuclei can form. Therefore, circumstellar nucleation would be expected to occur more rapidly under non-LTE conditions than under LTE conditions.

Nuth et al. [2] attempted to apply the Rasmussen Theory to their results from the study of the condensation of Ag. The temperature at which nucleation occurred appeared to depend on the total pressure of the system: as the total pressure increased, the nucleation of Ag became easier. The Rasmussen Theory did not fit the Ag nucleation data if the constant K from eqn.(1.7) was assigned the value of 1.25. Although Rasmussen [7] does refer to K as a "universal" constant, he does suggest that K may not always be universal, and that it could depend on the system studied. Once again, not enough experimental data are available to prove or disprove Rasmussen's adjustment to the Classical Theory.

1.4. Scope of this Study

The mechanisms by which refractory materials nucleate have yet to be determined. Neither the Classical Theory nor the Rasmussen Theory appear to agree with the experimental data collected so far; therefore, much more data need to be collected before these mechanisms can be fully understood. As was noted earlier, silicon oxide and silver have already been studied. However, several problems occurred during these experiments which could have affected the results significantly. First, the high temperature difference between the crucible and the ambient gas atmosphere in the chamber may have produced thermal convection which would have an effect on the uniformity of condensation during the experiment. Second, soon after the clusters form and begin to grow, they begin to settle out of the atmosphere due to their higher density. Therefore, the study of the growth and coagulation of these particles is difficult in earth's gravitational field.

NASA is in the process of designing a series of experiments to overcome these and other problems associated with nucleation studies of refractory vapors in terrestrial cloud chamber experiments. These experiments will study the homogeneous nucleation in a microgravity environment of a number of species, starting with magnesium, tin and lead. The first system to be studied will be magnesium vapor diffusing through and condensing in an argon atmosphere. The experimental apparatus will be tested on the KC-135 research aircraft which can fly parabolic trajectories so that microgravity conditions can be obtained for approximately twenty-five second periods.

The objective of my thesis is to develop a mathematical model for

the development of the temperature profile and the concentration profile of diffusing vapor species. The mathematical model will be used to identify conditions under which nucleation is likely to occur. The results from the mathematical model will also be helpful for selecting the test chamber design.

The mathematical model will be developed for two concentric spheres. The inner small spherical surface will represent the hot source, and the outer sphere will be the sink. Convection and radiation will be neglected, and only transfer by conduction and molecular diffusion will be considered. First, the development of a steady temperature profile is determined for this spherical geometry. Two temperature distributions will be studied: the steady state temperature profile assuming a constant thermal diffusivity, and a steady state temperature profile using the temperature dependent thermal diffusivity. An important result is the time required to achieve a steady temperature distribution.

Once a steady temperature profile is established, the temperature dependence of the molecular diffusion coefficient of the vapor can be determined, and the developing partial pressure profile can be calculated. The local equilibrium vapor pressure is calculated from the temperature profile using an Antoine-type equation. Since the vapor pressure decreases exponentially with decreasing temperature, relatively high supersaturation ratios can be expected away from the hot source. Finally, the supersaturation ratio will be calculated for different boundary conditions to determine its sensitivity to changes of each parameter in the equations developed for the hollow sphere model.

Chapter 2
THEORETICAL MODEL

The purpose of developing a mathematical model to calculate the supersaturation ratio is not to predict where nucleation will occur, but rather to calculate a range of values in which the supersaturation ratio is large enough for the onset of nucleation to occur at rates where condensation can be visually observed. Based on previous studies, this would require nucleation rates on the order of 10^9 - 10^{11} particles/cm^3/s [1,2].

A mathematical model will be developed for a hollow sphere geometry to calculate a range of supersaturation ratio values. In order to do this, a temperature distribution needs to be established so that the partial pressure and vapor pressure of a species at a particular point can be calculated. Two temperature distributions will be developed and then examined in Chapter 4. One temperature distribution uses a constant thermal diffusivity, while the other one accounts for the temperature dependency of the thermal diffusivity.

2.1. Development of the Mathematical Model

The hollow sphere model (see Fig. 2-1) was chosen because it is a relatively simple geometry for which solutions of the governing equations with various boundary conditions are readily available. Even though the experimental apparatus is to be cylindrical in shape, the profiles developed

by both the model and the experiments can be expected to be similar close to the hot source. However, the model is not expected to be very good closer to the outer sphere. Since a previous study reported that nucleation occurred relatively close to the hot source, the hollow sphere model should simulate the actual experiment. The developed equations are used to determine

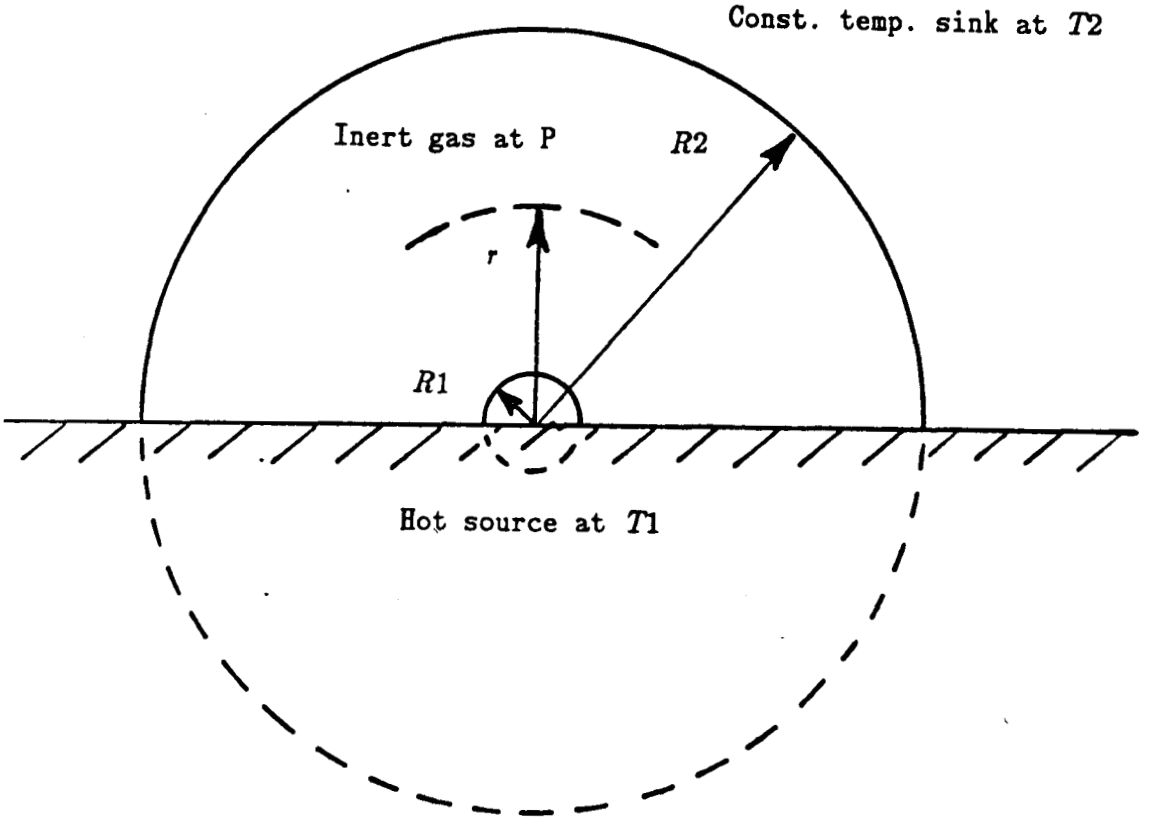

Figure 2-1: Hollow Sphere Model

whether or not supersaturation ratios large enough to induce homogeneous nucleation can be obtained within the time available for experimental runs aboard the KC-135 aircraft.

The supersaturation ratio, S, is defined as the ratio of the partial pressure of the material, Pp, to the vapor pressure of the material, Pv, at a specific point:

$$S = \frac{Pp}{Pv} \tag{2.1}$$

The vapor pressure is usually calculated using the Antoine equation:

$$\log(Pv) = A_v - \frac{B_v}{T} \tag{2.2}$$

where T has units of degrees Kelvin, Pv has units of torr and A and B are constants for a given substance.

2.1.1. Temperature Profile: Constant Thermal Diffusivity

A temperature distribution needs to be developed so that the vapor pressure can be calculated at a specific point. The general equation used to calculate the temperature profile is:

$$\frac{\partial T}{\partial t} = \alpha\left(\frac{\partial^2 T}{\partial r^2} + \frac{2\partial T}{r\partial r}\right) \tag{2.3}$$

where α is the thermal diffusivity, with units of cm^2/s, and is assumed to be constant.

The boundary conditions for the hollow sphere model are:

for $t < 0$

and $R1 \leq r \leq R2 \quad T = T_o$;

for $t \geq 0$

and $r = R1 \quad T = T1$

$r = R2 \quad T = T2$

The general solution of eqn.(2.3) is given by Crank [14, p.99]. Letting $T_o = T2$, this solution becomes:

$$T = \frac{R1T1}{r} + \frac{(R2T2 - R1T1)(r - R1)}{r(R2 - R1)} + \frac{2}{r\pi}\sum_{n=1}^{\infty} \frac{R2T2\cos(n\pi) - R1T1}{n} \sin\frac{n\pi(r - R1)}{R2 - R1} \exp\left(\frac{-\alpha n^2\pi^2 t}{(R2 - R1)^2}\right) \tag{2.4}$$

If we subtract $T2$ from both sides of eqn.(2.4) so that the system is in terms of the excess temperature, $T_{ex} = T - T2$, then eqn.(2.4) becomes:

$$T_{ex} = \frac{R1(R2 - r)(T1 - T2)}{r(R2 - R1)} - \frac{2R1(T1 - T2)}{r\pi} \times \sum_{n=1}^{\infty} \frac{1}{n} \sin\frac{n\pi(r - R1)}{R2 - R1} \exp\left(\frac{-\alpha n^2\pi^2 t}{(R2 - R1)^2}\right) \tag{2.5}$$

At steady state, eqn.(2.5) becomes

$$T_{ex} = (T1 - T2)\frac{R1(R2-r)}{r(R2-R1)} \tag{2.6}$$

2.1.2. Temperature Profile: Temperature Dependent Thermal Diffusivity

The steady state temperature profile developed in Section 2.1.1 assumed thermal diffusivity to be constant. To incorporate the temperature effect on the thermal diffusivity α, Crank [14, p.160] suggested the following procedure.

At steady state the basic equation used to calculate the temperature profile is given by:

$$\frac{d}{dr}\alpha(T)\frac{dT}{dr} = 0 \tag{2.7}$$

With boundary conditions for the hollow sphere model the same as in Section 2.1.1, the resulting solution of eqn.(2.7) is of the form:

$$\frac{R2(R1-r)}{r(R1-R2)} = \frac{T1+F(T1)-T-F(T)}{T1+F(T1)-T2-F(T2)} \tag{2.8}$$

where:

$$F(T) = \int_0^T f(T')dT' \tag{2.9}$$

The function, $f(T)$, can be obtained from the relationship:

$$\alpha = \alpha_o(1 + f(T)) \tag{2.10}$$

and is therefore:

$$f(T) = \frac{\alpha}{\alpha_o} - 1 \tag{2.11}$$

The thermal diffusivity is assumed to be that of the ambient inert gas since the diffusing vapor concentrations are too low to affect the thermal diffusivity significantly. If the ambient gas is argon, then an empirical relationship for the thermal diffusivity can be determined (see Appendix B):

$$\alpha_{Ar} = 8.32\times10^{-3}\frac{T^{1.73}}{P} \tag{2.12}$$

If we let $\alpha = \alpha_o$ at $T = T2$ and $P = 760$ torr, then

$$\alpha_o = \frac{8.32\times10^{-3}}{760}\, T2^{1.73} \tag{2.13}$$

Substituting eqn.(2.12) and eqn.(2.13) into eqn(2.11), we get

$$f_{Ar}(T) = \frac{760\,T^{1.73}}{P\,T2^{1.73}} - 1 \tag{2.14}$$

Eqn.(2.14) can be placed in terms of T_{ex} = T - $T2$, so that eqn.(2.9) can be written as

$$F(T_{ex}) = \int_0^{T_{ex}} (\frac{760}{P}(\frac{T_{ex}'}{T2} + 1)^{1.73} - 1) dT_{ex}' \tag{2.15}$$

Therefore,

$$F(T_{ex}) = \frac{760T2}{2.73P}((\frac{T_{ex}}{T2} + 1)^{2.73} - 1) - T_{ex} \tag{2.16}$$

Eqn.(2.8) can also be placed in terms of excess temperature so that

$$\frac{R2(R1 - r)}{r(R1 - R2)} = \frac{T_{ex,1} + F(T_{ex,1}) - T_{ex} - F(T_{ex})}{T_{ex,1} + F(T_{ex,1}) - T_{ex,2} - F(T_{ex,2})} \tag{2.17}$$

where

$$
\begin{aligned}
T_{ex} &= T - T2 \\
T_{ex,1} &= T1 - T2 \\
T_{ex,2} &= 0
\end{aligned}
$$

If we plug $T_{ex,1}$ into eqn(2.16), then

$$F(T_{ex,1}) = \frac{760T2}{2.73P}((\frac{T1}{T2})^{2.73} - 1) - T1 + T2 \tag{2.18}$$

Likewise, if we plug $T_{ex,2}$ into eqn.(2.16), then

$$F(T_{ex,2}) = 0 \tag{2.19}$$

Substitution of eqn.(2.16), eqn.(2.18) and eqn(2.19) into eqn.(2.17) simplifies to:

$$\frac{R2(R1 - r)}{r(R1 - R2)} = \frac{Y - Z}{Y - 1} \tag{2.20}$$

where

$$Y = (\frac{T1}{T2})^{2.73} \tag{2.21}$$

and

$$Z = (\frac{T}{T2})^{2.73} \tag{2.22}$$

Finally, eqn.(2.20) can be solved for the temperature generating a temperature profile that incorporates the effect of the steady state temperature on the thermal diffusivity.

$$T = T2(Y - WX)^{0.37} \tag{2.23}$$

where

$$W = \frac{R1R2}{(R1 + r)(R1 - R2)} - \frac{R2}{(R1 - R2)} \tag{2.24}$$

and

$$X = Y - 1 \tag{2.25}$$

Now, eqn.(2.23) can be used to calculate a new temperature profile. This profile will be compared with the temperature profile obtained from eqn.(2.6), and the effect that each equation has on the partial pressure profile and the supersaturation ratio will be compared in Chapter 4.

2.1.3. Partial Pressure Profile

The general equation used to calculate the concentration profile in spherical geometry is

$$\frac{\partial C}{\partial t} = D\left(\frac{\partial^2 C}{\partial r^2} + \frac{2\partial C}{r\partial r}\right) \tag{2.26}$$

where D is the molecular diffusion coefficient with units of cm^2/s and is assumed to be a function of temperature and pressure only.

The boundary conditions for the hollow sphere model are

for $t < 0$

and $R1 \leq r \leq R2 \quad C = C_o = C2$;

for $t \geq 0$

and $r = R1 \quad C = C1$

$r = R2 \quad C = C2$

If the same procedure is used for the concentration profile as was used for the temperature profile developed in Section 2.1.1, then the solution to eqn.(2.26) is:

$$C = \frac{R1C1}{r} + \frac{(R2C2 - R1C1)(r - R1)}{r(R2 - R1)} -$$

$$\frac{2}{r\pi}\sum_{n=1}^{\infty} \frac{R1(C1 - C2)}{n} \sin\frac{n\pi(r - R1)}{R2 - R1} \exp\left(\frac{-Dn^2\pi^2 t}{(R2 - R1)^2}\right) \tag{2.27}$$

With C in the dimensionless form:

$$C^* = \frac{C - C2}{C1 - C2}$$

eqn.(2.27) becomes:

$$C^* = \frac{R1(R2-r)}{r(R2-R1)} - \frac{2R1}{r\pi}\sum_{n=1}^{\infty}\frac{1}{n}\sin\frac{n\pi(r-R1)}{R2-R1}\exp\left(\frac{-Dn^2\pi^2t}{(R2-R1)^2}\right) \tag{2.28}$$

At moderate temperatures and pressures, the ideal gas law can be used to put eqn.(2.28) in terms of partial pressure.

$$Pp^* = \frac{R1(R2-r)}{r(R2-R1)} - \frac{2R1}{r\pi}\sum_{n=1}^{\infty}\frac{1}{n}\sin\frac{n\pi(r-R1)}{R2-R1}\exp\left(\frac{-Dn^2\pi^2t}{(R2-R1)^2}\right) \tag{2.29}$$

The only part of eqn.(2.29) which is dependent on the temperature and pressure of the system is the diffusion coefficient, D. The general relation used to calculate the diffusion coefficient for a binary gaseous mixture of A and B is

$$D_{A-B} = 1.858\times10^{-3}\frac{T^{1.5}(M_A+M_B)^{0.5}}{P\sigma^2{}_{A-B}\Omega_D(M_AM_B)^{0.5}} \tag{2.30}$$

Calculation of $D_{A\text{-}B}$ is shown in Appendix C [15].

Now, eqn.(2.6) or eqn.(2.23) and eqn.(2.29) are used to simulate the

movement of the diffusing material through an inert atmosphere. Then, combining these equations with eqn.(2.2) and eqn.(2.1), the range of supersaturation ratios at different time intervals can be calculated throughout the experimental chamber.

2.2. Parameters Affecting the Mathematical Model

Many parameters in eqn.(2.2), eqn.(2.6), eqn.(2.23) and eqn.(2.29) have an effect on the supersaturation ratio: the temperature profile, total pressure, radii of the inner and outer spheres, and the inert gas atmosphere. Any one of these parameters may have a significant effect on the supersaturation ratio or no effect at all.

The temperature profile can be changed directly by raising or lowering the temperature at the inside boundary ($T1$) or at the outside boundary ($T2$). The profile can also be changed indirectly by increasing or decreasing the size of the inner sphere ($R1$) or by increasing or decreasing the distance to the outside boundary ($R2$). Since both the partial pressure and the vapor pressure are dependent on the temperature at a particular location, it is difficult to determine the overall effect which $T1$, $T2$, $R1$ and $R2$ have on the supersaturation ratio. Whichever pressure, Pp or Pv, is affected more by a change in temperature will determine whether the supersaturation ratio will increase or decrease at a specific location.

Total pressure apparently has no effect on the temperature profile, but does affect the rate of molecular diffusion through the ambient gas. Therefore, with a lower total pressure at a given temperature, the vapor pressure will remain the same, but the rate at which the vapor diffuses will increase which will in turn increase the partial pressure and consequently

raise the supersaturation ratio at that specific location. Likewise, the supersaturation ratio should decrease when the total pressure is increased and the temperature remains constant.

A similar effect should be seen if the inert ambient gas is changed. The higher the molecular weight of the inert gas, the slower the diffusion through the ambient gas. The partial pressure will then be decreased and the supersaturation ratio will be lowered. The opposite will occur if a lower molecular weight inert gas is used.

The above simple mathematical model can be used to predict the effect which each parameter has on the supersaturation ratio so that the experiments can be run successfully. A successful experiment means that nucleation occurs within the allotted time interval and far enough away from the source of the vapor for accurate experimental determination of the point of nucleation. Granted, the model cannot predict the exact location of nucleation without having the critical supersaturation ratio specified, but it does permit the identification of the conditions likely to produce ranges of supersaturation ratios where it is believed that nucleation should occur. It can also be used to evaluate suggestions as to what to change to force nucleation if it did not occur initially. Should $T1$ be raised or lowered? What about $T2$? Will changing the pressure have an effect on nucleation? From this study, conditions under which the experiments should be run will be determined.

2.3. Limitations of the Hollow Sphere Model

It must be noted that once nucleation begins, these equations may no longer be useful because other factors become involved in the process. The most significant of these is probably the rate of growth of the nucleus. Once the energy barrier that prevents spontaneous nucleation is overcome, the growth rate of the nucleus becomes very fast. As the nucleus grows in size, the partial pressure in the neighborhood of the solid particle will decrease accordingly. Neither the diffusion equation nor the temperature equation can be used to determine the particle growth rate.

Very little vapor is likely to diffuse past the nucleus and travel towards the outside barrier due to the greater possibility that the nucleus and the vapor molecules will collide and stick together. The diffusion equation is used only to predict the rate at which vapor molecules move through the inert atmosphere and does not take into account the interaction between the nucleus and the vapor molecules; therefore, once nucleation occurs, the diffusion equation can no longer be expected to predict the movement of vapor molecules through the inert atmosphere with much confidence.

The temperature profile in the region where nucleation begins will be affected by the energy released when condensation occurs. This energy, the heat of condensation, could be used to estimate the change in temperature near the site of nucleation. If the temperature is increased significantly, then both the vapor pressure and the partial pressure will be affected by the release of energy during condensation.

Also, the effects of thermal radiation on the temperature profile have

been omitted from this study; therefore, when the temperature is measured during the experiment, a certain amount of error is expected in the equations.

The geometry of the mathematical model is spherical, whereas the experimental apparatus is expected to be cylindrical in shape. Although the development of the profiles is expected to be similar for both geometries near the inner source, they could be vastly different near the outer boundary. As long as nucleation occurs relatively close to the inner source, the mathematical model should predict the range of conditions needed for nucleation to occur.

Chapter 3
EXPERIMENTAL

Before the experiments can be performed in zero gravity for an extended length of time, preliminary experiments must be performed to test the experimental apparatus in a microgravity environment. These experiments will be run on NASA's KC-135 research aircraft which can maintain zero gravity for approximately twenty-five seconds by flying a parabolic route. The aircraft will fly a number of parabolic trajectories during any one test flight so that a series of experiments can be completed. The initial trial runs will use a very simple system that will consist of a cylindrical container with a heated crucible at one end. A metal will be melted inside the crucible producing equilibrium vapor pressure over the molten surface. The vapors are then released to diffuse into the inert atmosphere in the cylindrical chamber at lower temperatures where condensation will take place. The experiments will be taped using a video cassette in order to determine where nucleation occurs. Since the experiments will only have available a time span of under twenty-five seconds, the study of the growth of the clusters will necessarily be limited. This aspect of study will be done at a later time when longer periods of microgravity become available. The experiments performed on the KC-135 research aircraft will be used primarily to develop an apparatus and measurement techniques and to determine the conditions under which nucleation occurs.

3.1. Materials to be Investigated

A variety of materials will be studied in order to gain a better understanding behind the nucleation phenomenon of refractory materials. A series of relatively simple metals will be investigated first before more complex materials will be examined. Magnesium will be the first metal to be studied in the new experimental apparatus. Nucleation of Mg vapor is expected to occur at very high supersaturation values because the Mg dimer is a van der Waals molecule. Because of the high degree of supersaturation needed to cause nucleation, the cloud of Mg clusters should have a sharp front and therefore should be relatively easy to locate.

Later, tin and lead may be studied in the same chamber. Tin vaporizes as a dimer and lead as a tetramer; therefore, lower degrees of supersaturation are expected for condensation of these metals than for magnesium. Also, the results from the experiments with tin and lead can be compared with the shock tube analysis by Bauer et al. [10,11].

3.2. Description of Experimental Apparatus

The experimental apparatus as now visualized will be cylindrical in shape and divided into two sections (see Fig. 3-1). The well-insulated top section contains the crucible where the metal is vaporized. The crucible is placed in the top section in an attempt to reduce convective instabilities between zero gravity periods arising from the temperature and density gradients in the cloud chamber. In this section, there is an upper heater and a lower heater (see Fig. 3-2). The upper heater surrounds the crucible and is used to control the vapor pressure of the metal inside and around the crucible.

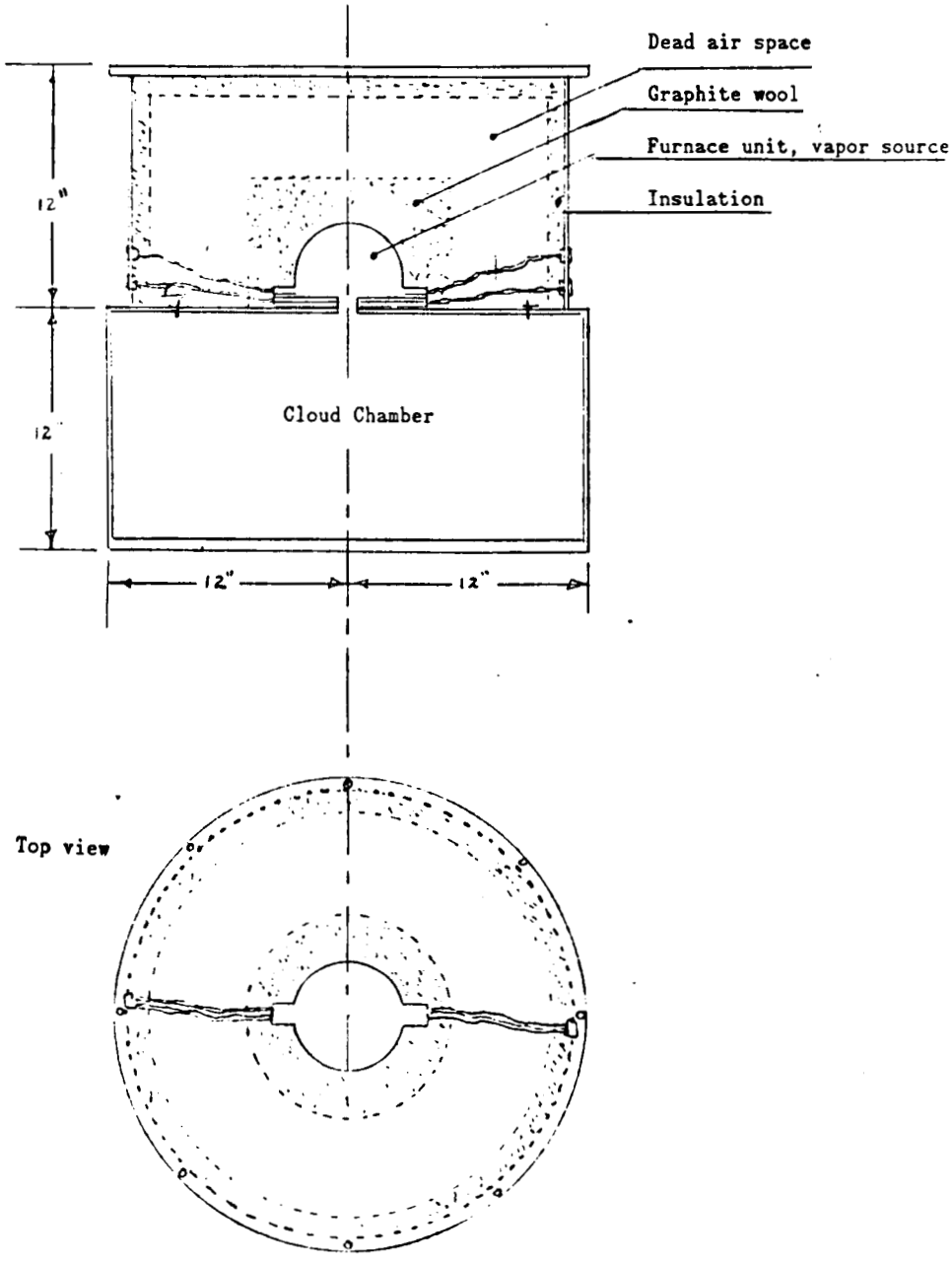

Figure 3-1: Proposed Experimental Apparatus

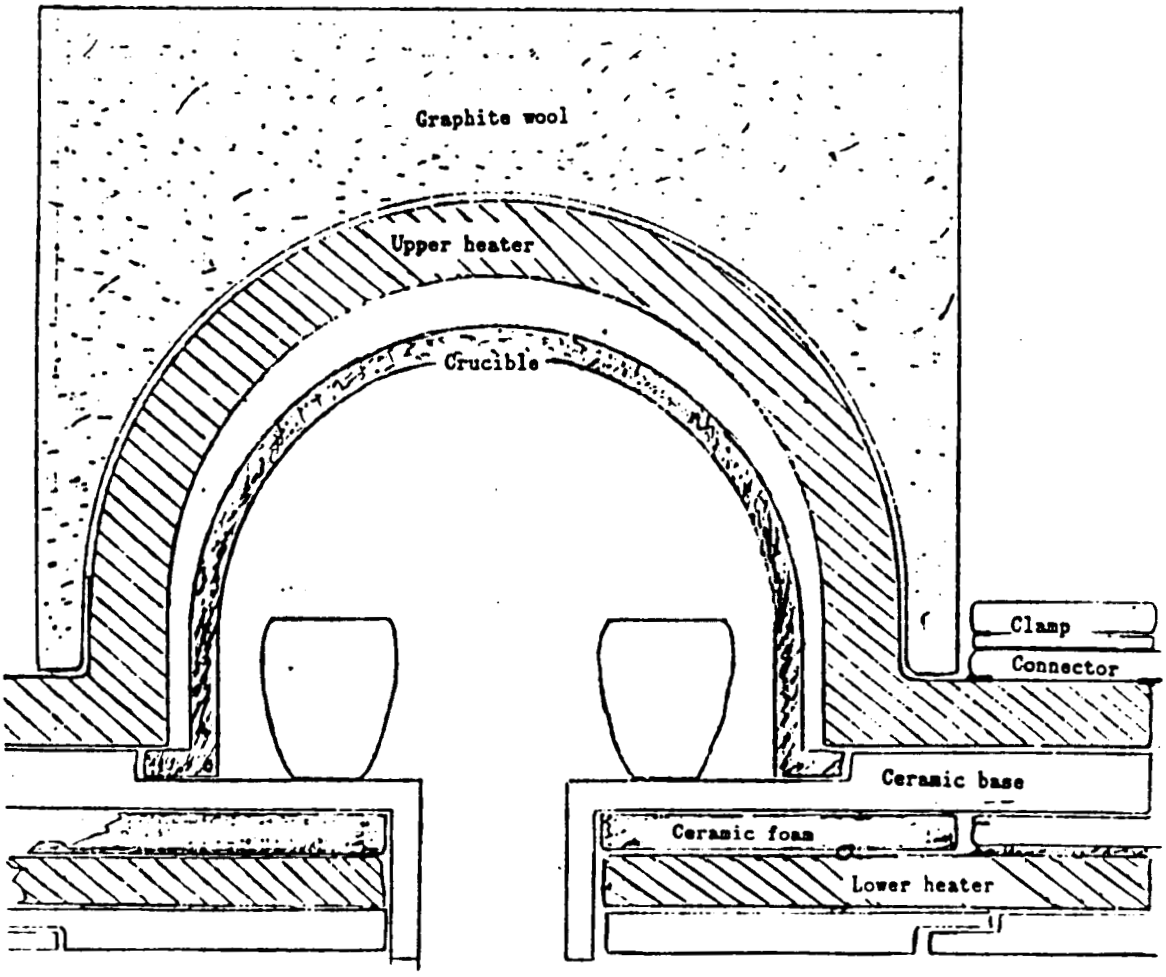

Figure 3-2: Proposed Apparatus: Top Section

The lower heater is approximately 4cm in radius and is used to control the temperature profile in the cloud chamber. A temperature at the lower heater which is higher than in the crucible should push the point of nucleation farther from the opening of the crucible and thus make it easier to locate. The rest of the top section is filled with graphite wool which serves as an insulator.

The bottom section of the apparatus will be referred to as the cloud chamber. This chamber is initially filled with an inert gas and maintained at a specific pressure. A steady temperature profile will be established dependent on the temperature of the hot crucible as the source and the temperature of the ambient atmosphere surrounding the chamber as the heat sink. When the experiment is ready to run, the metal vapor is released from the crucible into the cloud chamber by opening the cover on the crucible compartment. This is the section where nucleation occurs. The outside wall of the cloud chamber is made of a thick clear plastic so that the entire run can be video taped.

3.3. Experimental Procedure

The temperature of the crucible, the temperature of the ambient atmosphere and the total pressure in the cloud chamber will be fixed before the KC-135 research aircraft begins the ascent stage of the parabolic route. Thermocouples placed at strategic positions will monitor the temperature profile and determine when a steady temperature distribution has been achieved. When the KC-135 nears the peak of the parabola, the video

camera and the lights will be turned on. At this point, there will be a time delay, which will be varied throughout the flight, to allow for any convection currents to die out. The crucible compartment cover will then be removed and the metal vapor will diffuse into the cloud chamber. Nucleation will occur at a distance from the crucible at which the partial pressure of the diffusing vapor first exceeds the critical multiple of the vapor pressure (supersaturation ratio) of the same metal determined by the temperature at the point of nucleation.

The video tape of each run will be analyzed to determine the distance at which nucleation is first observed. Then the partial pressure of the metal vapor will be calculated using the model developed in Chapter 2. Hence, data for the partial pressure of the metal vapor needed to cause nucleation as a function of temperature can be generated. Finally, the supersaturation ratio will be calculated using the hollow sphere model and compared with past experimental results.

Chapter 4
RESULTS and DISCUSSION

The hollow sphere model developed in Chapter 2 will be used to generate data for the supersaturation ratio. The effect of each parameter on the temperature profile, the partial pressure profile and the supersaturation ratio will be studied. Since the actual temperature profile has not been determined, the effects on the supersaturation ratio of both temperature profiles developed in Chapter 2 will be examined. Also, a third possible temperature profile will be introduced and the effect that this profile will have on the supersaturation ratio will be predicted. Finally, the data generated from the hollow sphere model will be compared with existing experimental data.

A computer program (see Appendix D) was written to generate local supersaturation data using the following equations developed in Chapter 2:

$$T = (T1 - T2)\frac{R1(R2-r)}{r(R2-R1)} + T2 \qquad (2.6)$$

$$D_{Mg-Ar} = 4.877\times10^{-5}\frac{T^{1.5}}{P\Omega_D} \qquad (2.30)$$

$$Pp^* = \frac{R1(R2-r)}{r(R2-R1)} - \frac{2R1}{r\pi}\sum_{n=1}^{\infty}\frac{1}{n}\sin\frac{n\pi(r-R1)}{R2-R1}\exp\left(\frac{-Dn^2\pi^2t}{(R2-R1)^2}\right) \qquad (2.29)$$

$$\log(Pv) = A_v - \frac{B_v}{T} \tag{2.2}$$

$$S = \frac{Pp}{Pv} \tag{2.1}$$

The constants for eqn.(2.2) are listed in Appendix A. The expression for the diffusion coefficient is calculated in Appendix C.

Initially, the program was run at the following baseline conditions:

P = 760 torr
$T1$ = 1000 K
$T2$ = 293 K
$R1$ = 1.0 cm
$R2$ = 25.0 cm

Of course, once the experimental apparatus is built, $R1$ and $R2$ cannot be changed. We will, however, discuss the effects that both $R1$ and $R2$ have on the supersaturation ratio because these sizes had to be considered before the experimental apparatus was built.

It is believed that magnesium will need to reach a supersaturation ratio between 10^8 and 10^{11} in order for nucleation to occur. Therefore, we will determine under what combination of conditions such a supersaturation ratio range can be obtained and which parameters have the greatest effect on the likely nucleation. Each parameter will be considered separately; when one parameter is changed all other parameters will have the same value as for the baseline conditions.

4.1. Steady State Temperature Profile

This section is used to determine the effects of each parameter on the partial pressure profile calculated by eqn.(2.29) and the supersaturation ratio calculated by eqn.(2.1) using the constant α steady state temperature profile calculated by eqn.(2.6). The data generated by the computer program as a function of distance from the crucible were used to graph the steady state temperature profile, the partial pressure profile and the supersaturation ratio for varying times. These graphs are shown as Figure 4-1, Figure 4-2 and Figure 4-3 respectively. Since the total pressure and the inert gas do not affect the temperature profile, the effects of these parameters will be discussed in a later section. The parameters that do affect the temperature profile are $T1$, $T2$, $R1$ and $R2$. The figures in the following sections were arbitrarily chosen for t = 15 s.

4.1.1. Effect of the Crucible Temperature

As the value of $T1$ is increased, the temperature profile is greater close to the source and eventually approaches the same value as the distance from the source increases. The partial pressure increases as $T1$ increases because the partial pressure closest to the source is determined by the vapor pressure of the system at $T1$. Therefore, as $T1$ increases, the partial pressure is higher close to the source due to the dependence of the diffusion coefficient on the temperature (see eqn.(2.30)). Since the partial pressure profile is greater as $T1$ increases, there is a higher concentration gradient which causes the vapor molecules to diffuse at a faster rate than molecules at a lower temperature.

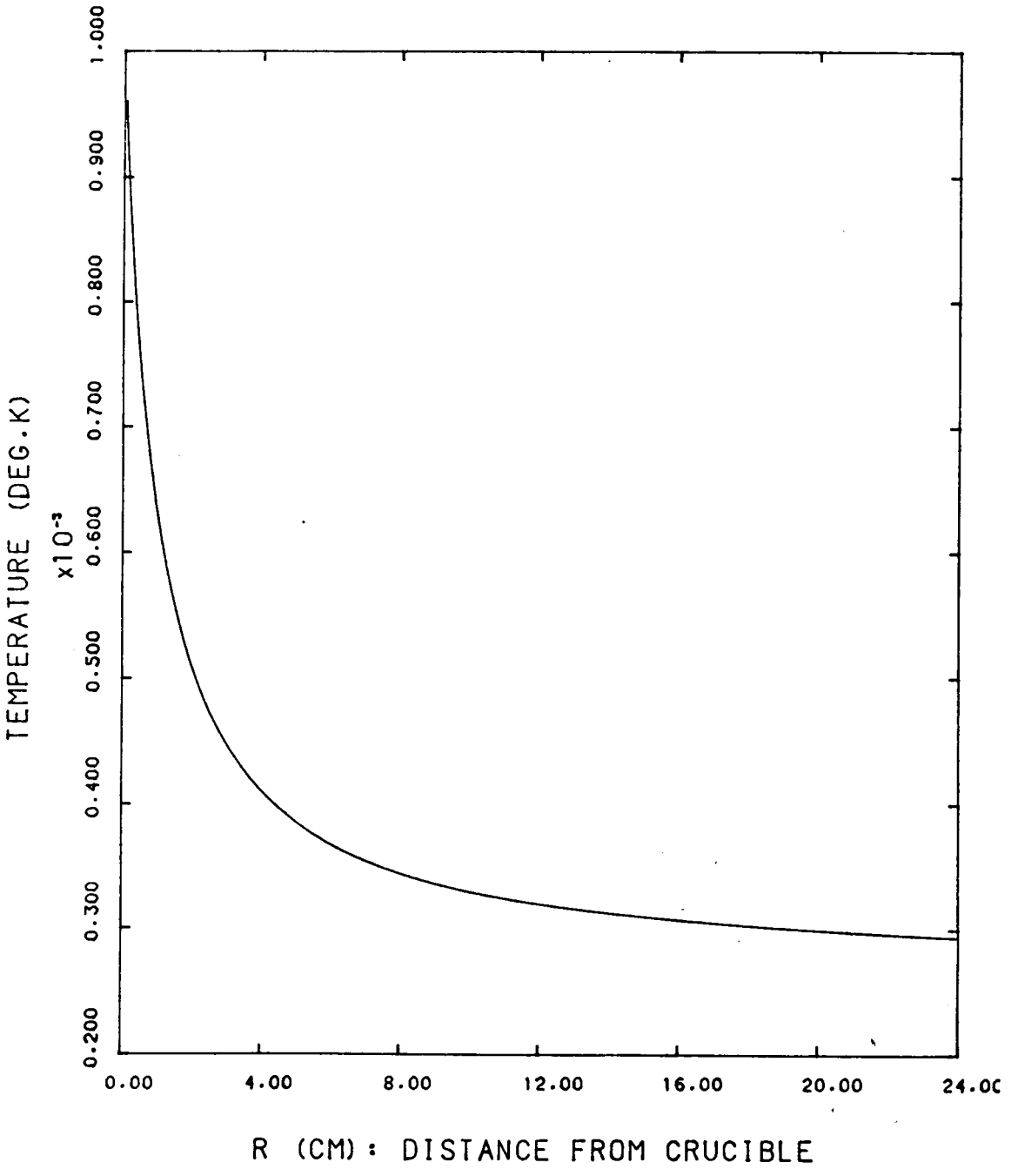

Figure 4-1: Temperature Profile: Baseline Conditions

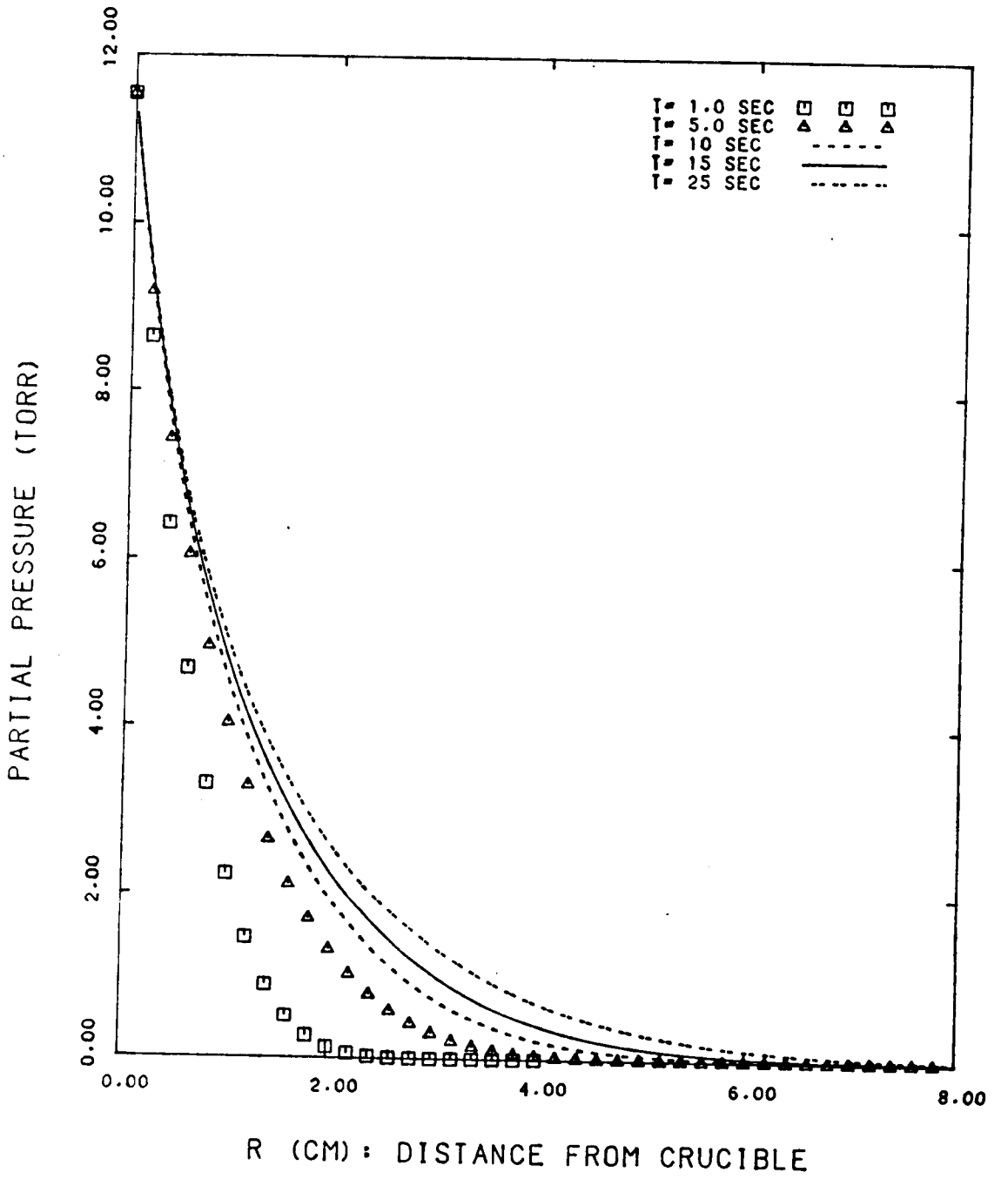

Figure 4-2: Partial Pressure Profile: Baseline Conditions

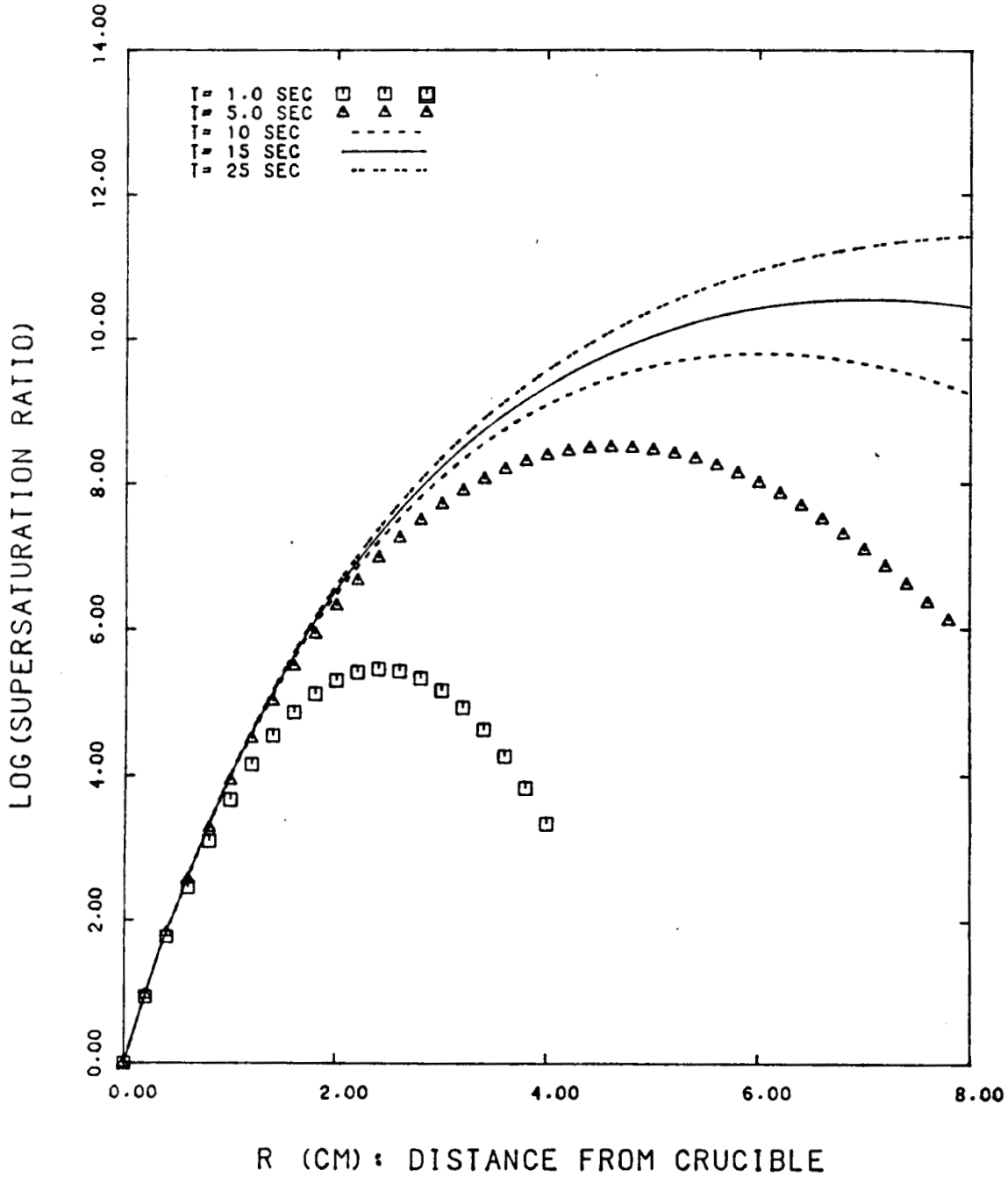

Figure 4-3: Supersaturation Ratio: Baseline Conditions

At early stages of profile development, the temperature has a greater effect on the vapor pressure than on the partial pressure; therefore, closer to the source the vapor pressure at 950 K is much less than the vapor pressure at 1200 K and the supersaturation ratio is lower closer to the source for higher $T1$. However, as the molecules diffuse away from the source, the temperature profiles are similar and the local vapor pressure with 950 K source approaches the vapor pressure with 1200 K source, but the partial pressure at 950 K is much less than the partial pressure at 1200 K; therefore, the supersaturation ratio is greater at distances farther from the source as $T1$ increases. This is shown by an increase in the maximum value and a shift of the maximum value away from the source in the S vs. r plot (see Figure 4-4).

4.1.2. Effect of the Ambient Temperature

As $T2$ is increased, the temperature profile becomes less steep closer to the source, and the difference between the curves increases as the difference in $T2$ increases. The temperature of the system is always greater for a greater $T2$. Likewise, both the partial pressure and the vapor pressure are increased throughout the system when $T2$ is increased. Since the vapor pressure increases exponentially with increasing temperature, the more the temperature is increased the lower the supersaturation ratio will be. Therefore, the supersaturation ratio decreases when $T2$ is increased. The distance at which the maximum value is reached is changed very slightly, but the actual maximum value is greatly reduced (see Figure 4-5).

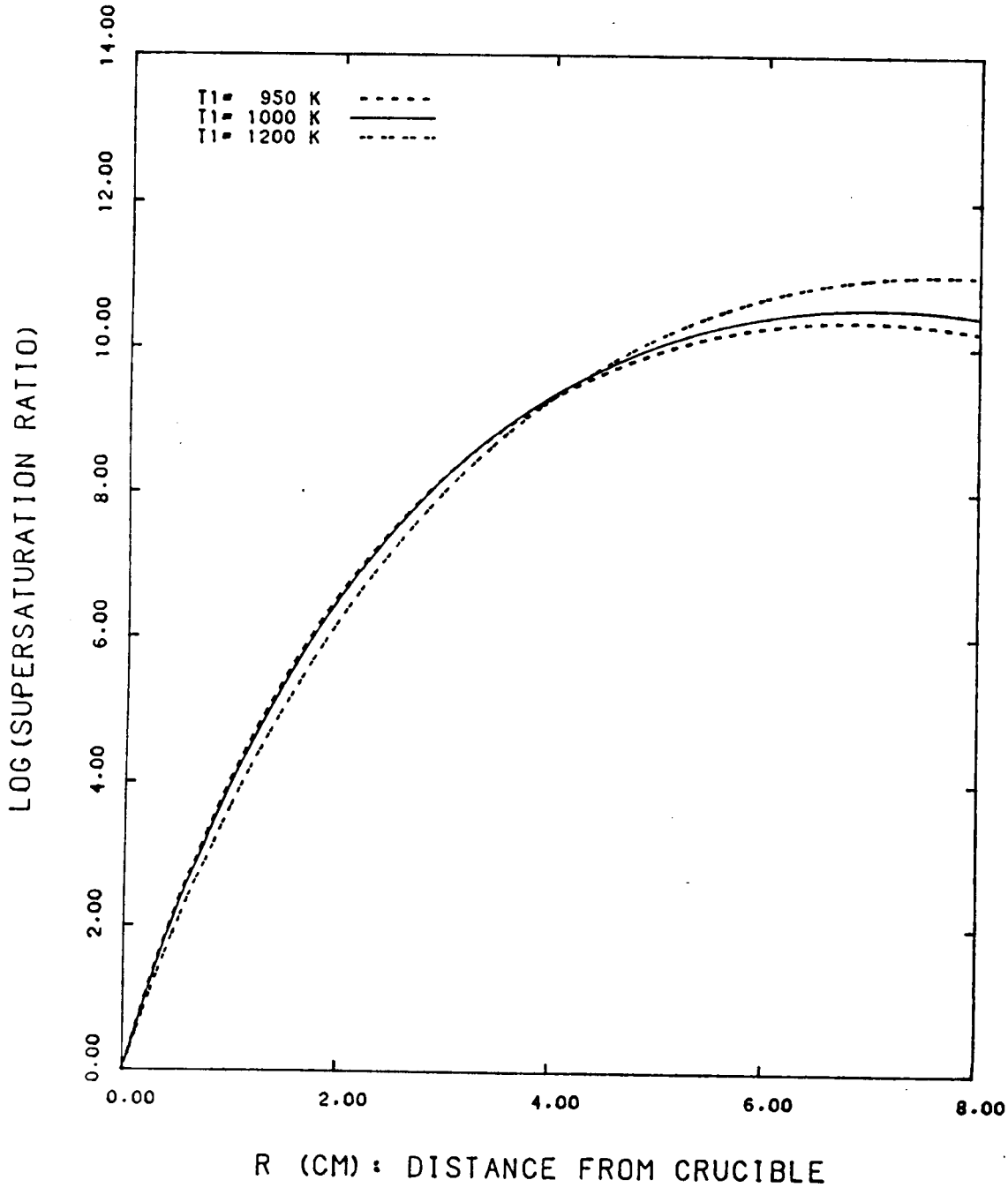

Figure 4-4: Effect of Crucible Temperature: t = 15 s

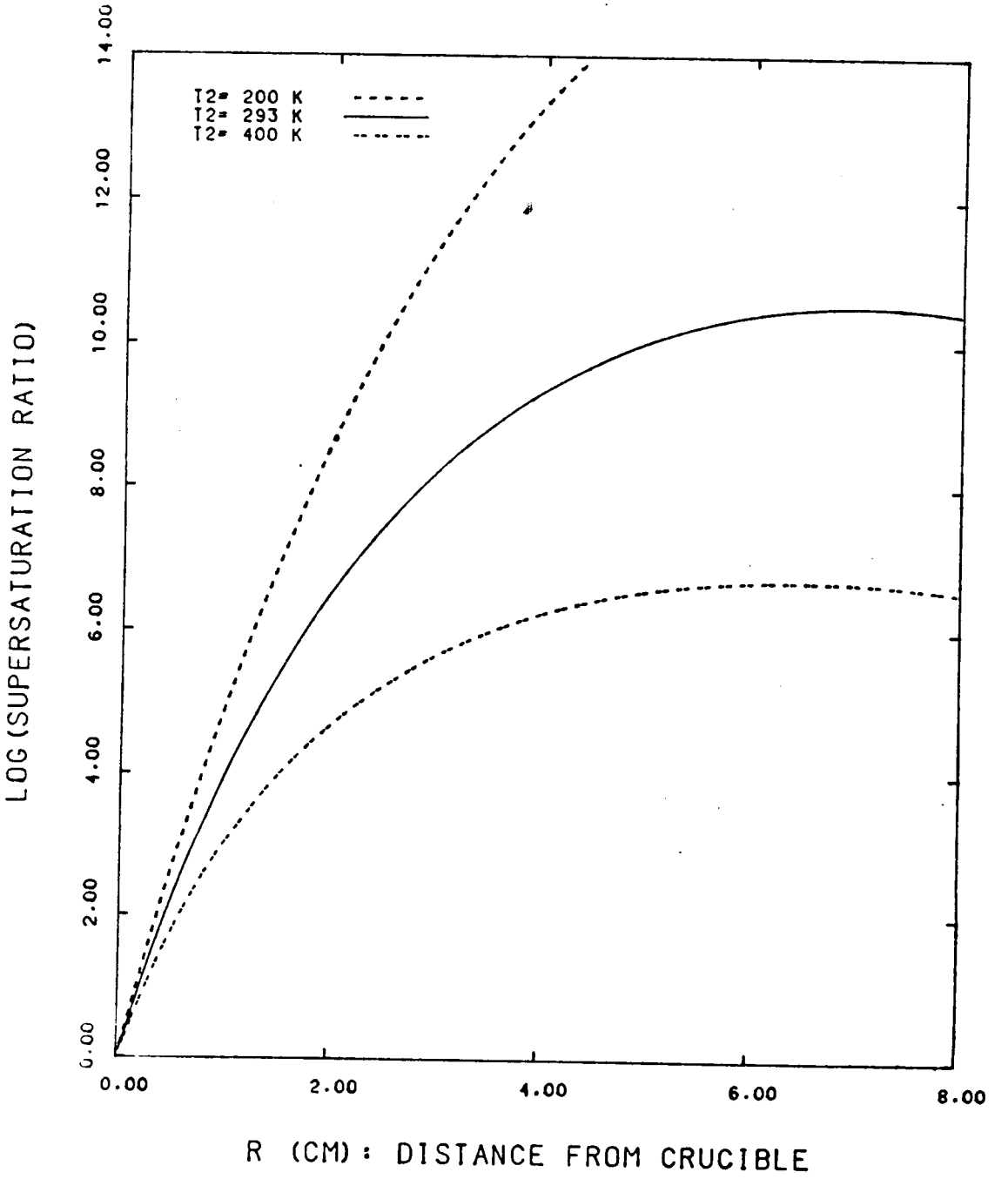

Figure 4-5: Effect of Ambient Temperature: t = 15 s

4.1.3. Effect of the Crucible Radius

As $R1$ is increased, the temperature profile becomes less steep closer to the source and the inert gas temperature is raised throughout the system. Likewise, the vapor molecules diffuse at a faster rate and the partial pressure is again increased. Since the temperature increases with increasing $R1$, the vapor pressure increases and the supersaturation ratio is decreased. Also, the system reaches a maximum value at a slower rate and the maximum value is lowered (see Figure 4-6).

4.1.4. Effect of the Outside Boundary

There is very little change in the temperature profile as $R2$ is increased. Likewise, the partial pressure is increased by a very small amount. Since the partial pressure remains essentially the same as $R2$ is increased, the primary change in the supersaturation ratio is due to the increase in temperature. The vapor pressure is increased due to the temperature increase; therefore, the supersaturation ratio is decreased as $R2$ is increased. The maximum value is lowered, but the distance from the crucible remains essentially the same (see Figure 4-7).

4.2. Comparison of the Temperature Profiles

The steady state temperature profile calculated by eqn.(2.6) does not take into account the effect of temperature on the thermal diffusivity. Intuitively, one would expect that the thermal diffusivity should have an effect on the temperature profile as shown by eqn.(2.23). Since it will not be known which temperature profile is more accurate until the experiments are run, both temperature profiles are considered.

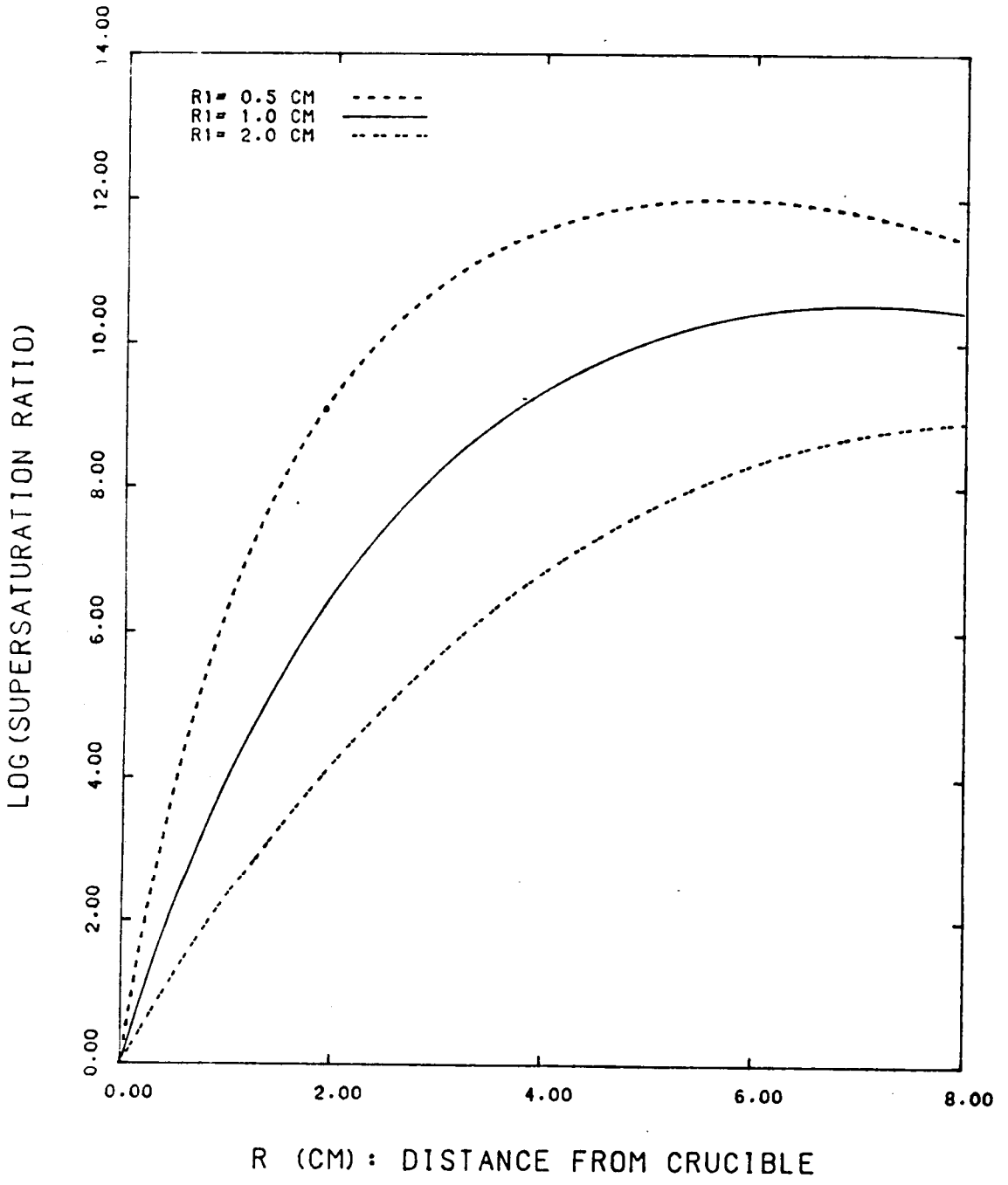

Figure 4-6: Effect of Crucible Radius: t = 15 s

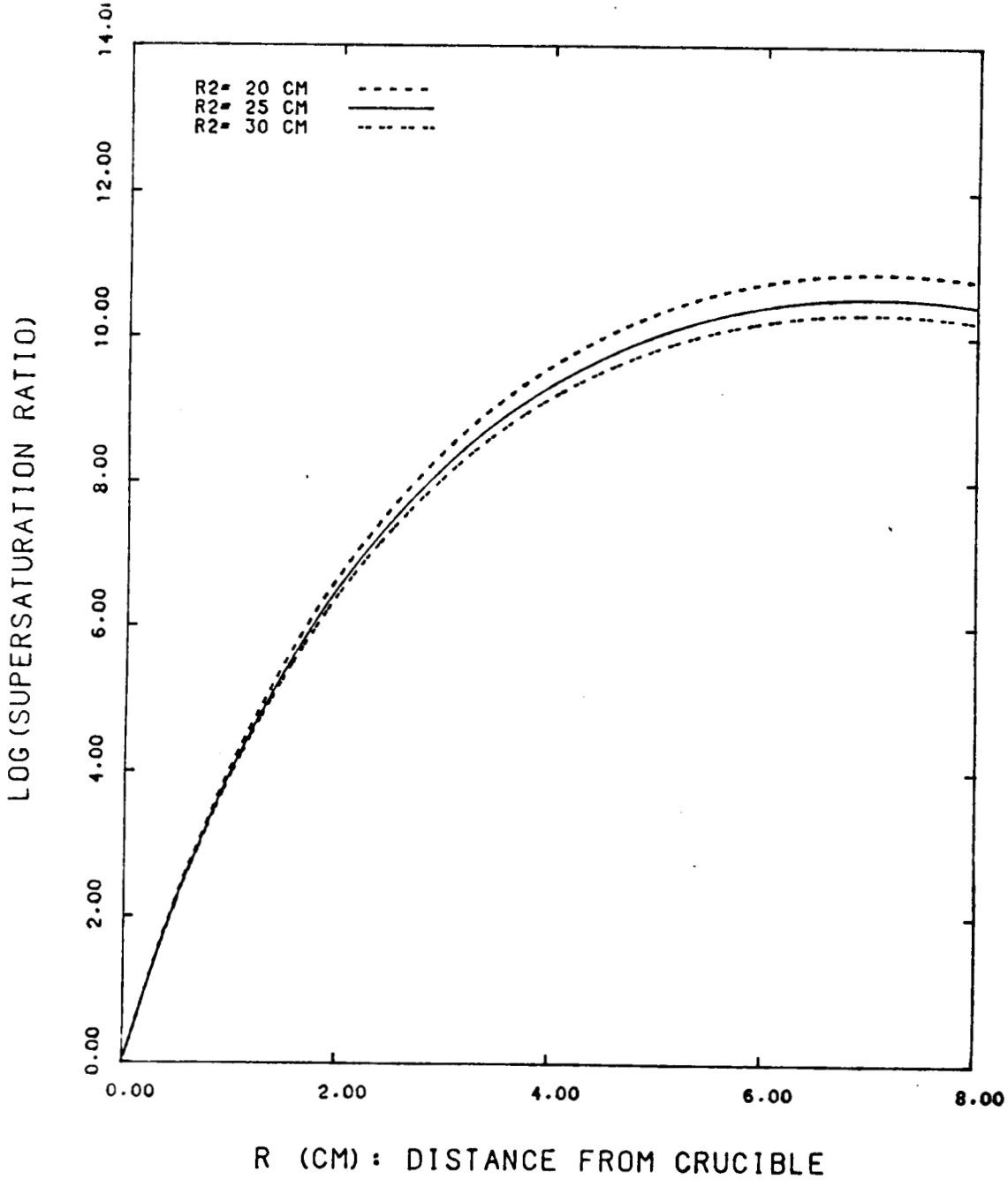

Figure 4-7: Effect of Outside Boundary: t = 15 s

Figure 4-8 shows that the temperature would be increased when the temperature dependent thermal diffusivity is considered. This means that the partial pressure and the vapor pressure are both increased throughout the chamber. Since the vapor pressure has a greater temperature dependence than the partial pressure, the supersaturation ratio is decreased when the temperature dependent thermal diffusivity is used (see Figure 4-9). Likewise, each parameter affects the supersaturation ratio in the same manner as was discussed when using the constant α steady state temperature profile except the supersaturation ratios are lower for the new temperature profile (compare Figure 4-9 with Figure 4-3).

Tables 4-1 and 4-2 show the time and distance at which the supersaturation ratio first equals 10^8, 10^9, 10^{10} and 10^{11} for each parameter change and for both temperature profiles. It is much more likely for the system to reach supersaturation ratios of 10^{10} or 10^{11} if the constant α steady state temperature profile were the more correct one, than when the temperature profile incorporated the temperature dependent thermal diffusivity. This is due to the faster rate at which the steady state temperature declines, which causes a lower vapor pressure, at a faster rate than the temperature profile adjusted by the effect of the thermal diffusivity.

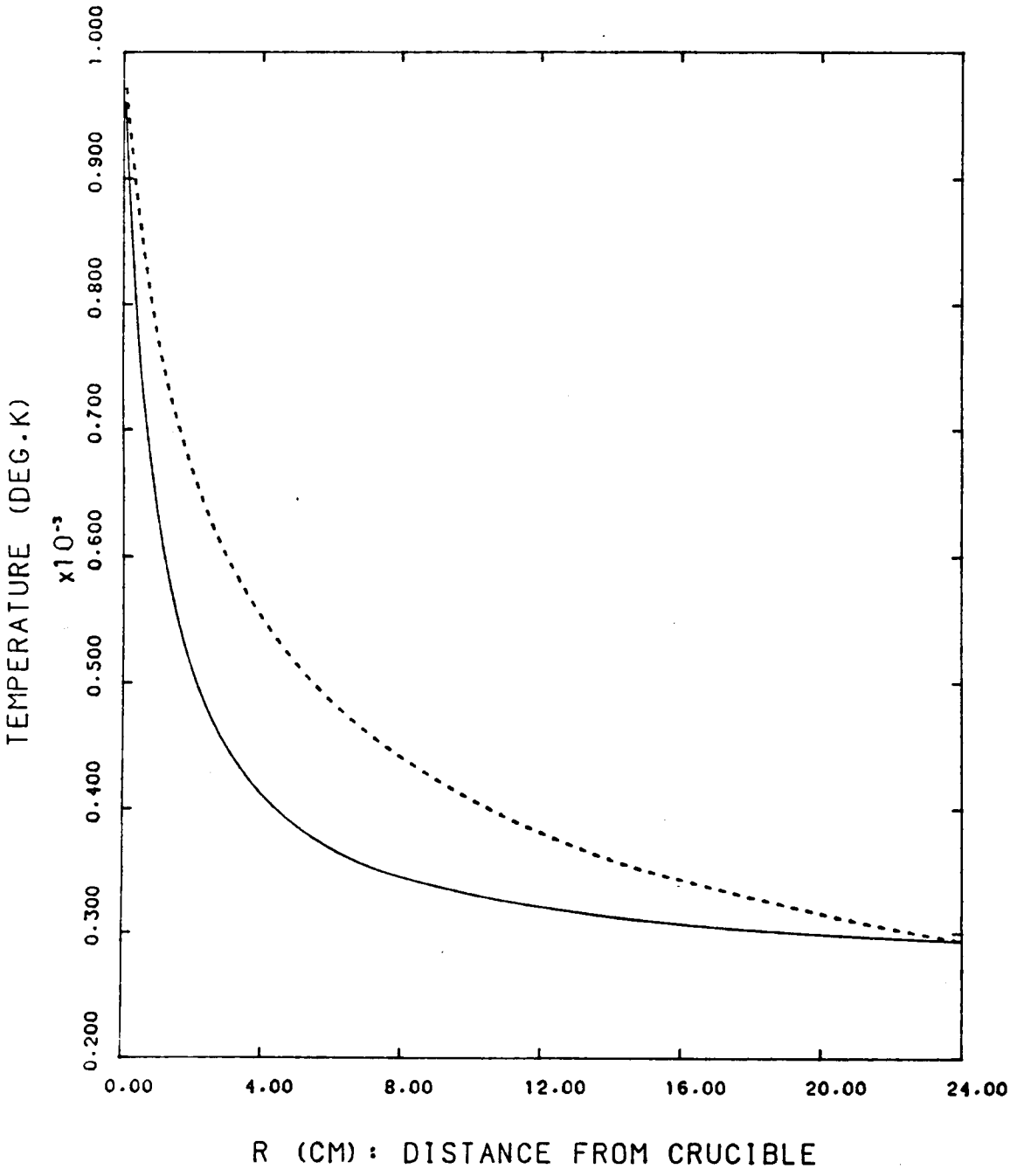

Figure 4-8: Comparison of Temperature Profiles

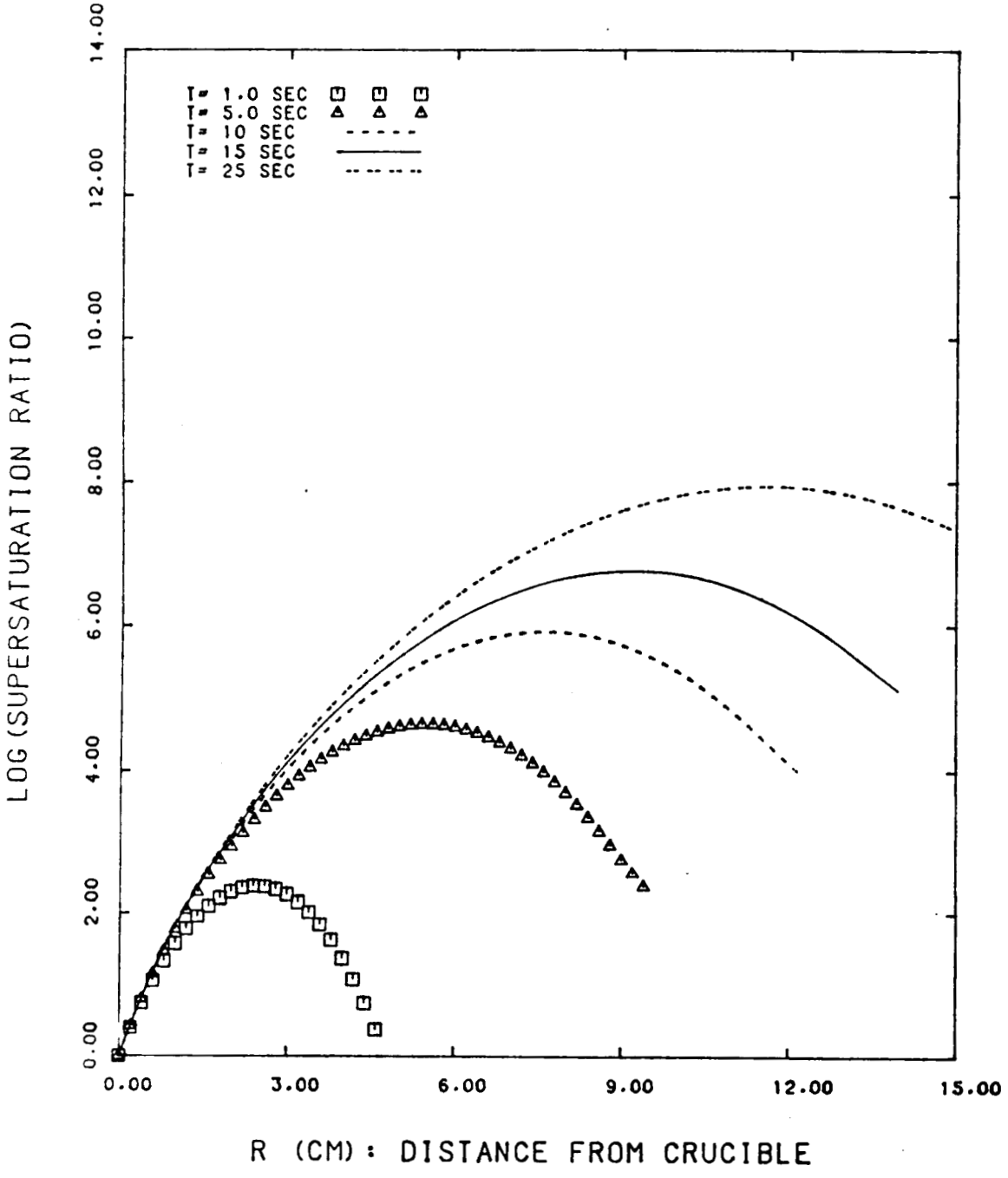

Figure 4-9: Supersaturation Ratio: variable α

Table 4-1: Parameter Effect on S: constant α

Unless otherwise stated, the parameters have the baseline values:

P = 760 torr
T1 = 1000 K
T2 = 293 K
R1 = 1.0 cm
R2 = 25.0 cm

The inert gas is Argon.
The temperature profile is calculated
assuming constant thermal diffusivity.
The distance from the source, r, is in cm.
The time, t, is in seconds.

Parameter values	$S = 10^8$ t	r	$S = 10^9$ t	r	$S = 10^{10}$ t	r	$S = 10^{11}$ t	r
baseline	4.0	4.0	7.0	4.6	12.0	5.6	20.0	7.2
R1=0.5	2.0	1.8	3.0	2.4	4.0	3.4	8.0	4.0
R1=2.0	10.0	6.8	16.0	7.8	25.0	9.2	----	---
R2=20.0	4.0	3.4	6.0	4.4	10.0	5.4	17.0	6.4
R2=30.0	5.0	3.6	8.0	4.6	13.0	6.0	23.0	7.4
P=250	2.0	3.2	3.0	4.0	4.0	5.6	7.0	6.8
P=1200	7.0	3.6	11.0	4.6	18.0	6.0	----	---
neon	3.0	3.4	4.0	4.4	6.0	6.0	11.0	6.8
krypton	6.0	3.6	9.0	5.0	16.0	5.8	27.0	7.4
T1=950	5.0	3.4	8.0	4.4	13.0	5.6	22.0	7.4
T1=1200	4.0	3.8	6.0	4.8	10.0	5.6	16.0	6.8
T2=200	2.0	2.2	2.0	2.8	3.0	3.0	4.0	3.6
T2=400	----	---	----	---	----	---	----	---

NOTE: "---" means that the value of S cannot be reached within 30 s.

Table 4-2: Parameter Effect on S: variable α

Unless otherwise stated, the parameters have the baseline values:

P = 760 torr
T1 = 1000 K
T2 = 293 K
R1 = 1.0 cm
R2 = 25.0 cm

The inert gas is Argon.
The temperature profile is calculated assuming temperature dependent thermal diffusivity.
The distance from the source, r, is in cm.
The time, t, is in seconds.

Parameter values	$S = 10^8$ t	r	$S = 10^9$ t	r	$S = 10^{10}$ t	r	$S = 10^{11}$ t	r
baseline	26.0	11.0	----	----	----	----	----	----
R1=0.5	12.0	7.0	21.0	8.0	----	----	----	----
R1=2.0	----	----	----	----	----	----	----	----
R2=20.0	20.0	9.8	28.0	11.8	----	----	----	----
R2=30.0	----	----	----	----	----	----	----	----
P=250	9.0	10.2	13.0	12.6	18.0	15.6	25.0	18.2
P=1200	----	----	----	----	----	----	----	----
neon	14.0	10.8	20.0	13.8	29.0	15.4	----	----
krypton	----	----	----	----	----	----	----	----
T1=950	26.0	10.4	----	----	----	----	----	----
T1=1200	28.0	12.6	----	----	----	----	----	----
T2=200	15.0	8.6	20.0	10.2	26.0	11.8	----	----
T2=400	----	----	----	----	----	----	----	----

NOTE: "---" means that the value of S cannot be reached within 30 s.

4.3. Effect of Total Pressure

As was stated earlier, the total pressure of the system is expected to have no effect on the steady temperature profile, but it does affect the partial pressure and hence the supersaturation ratio. Since the temperature is not changed, the vapor pressure is not affected; therefore, the only change in the supersaturation ratio is due to a change in partial pressure.

The diffusion rate, and therefore the partial pressure, decreases as the total pressure of the system is increased due to the inverse relationship between the diffusion coefficient and the total pressure. Since the vapor pressure remains the same for a given temperature, the supersaturation ratio will decrease as the total pressure is increased because the partial pressure is decreased. Also, the maximum value is reached closer to the source, but the maximum value decreases as the total pressure increases (see Figure 4-10).

4.4. Effect of Ambient Gas

The ambient inert gas in the test chamber affects the supersaturation ratio in much the same way as the total pressure. The higher the molecular weight of the ambient gas, the slower the rate at which the vapor molecules diffuse away from the crucible and the lower the partial pressure. Likewise, the supersaturation ratio will decrease due to the decrease in the partial pressure and no change in the vapor pressure. Once again, the maximum value is reached closer to the crucible, but the maximum value decreases as the molecular weight of the ambient gas increases (see Figure 4-11).

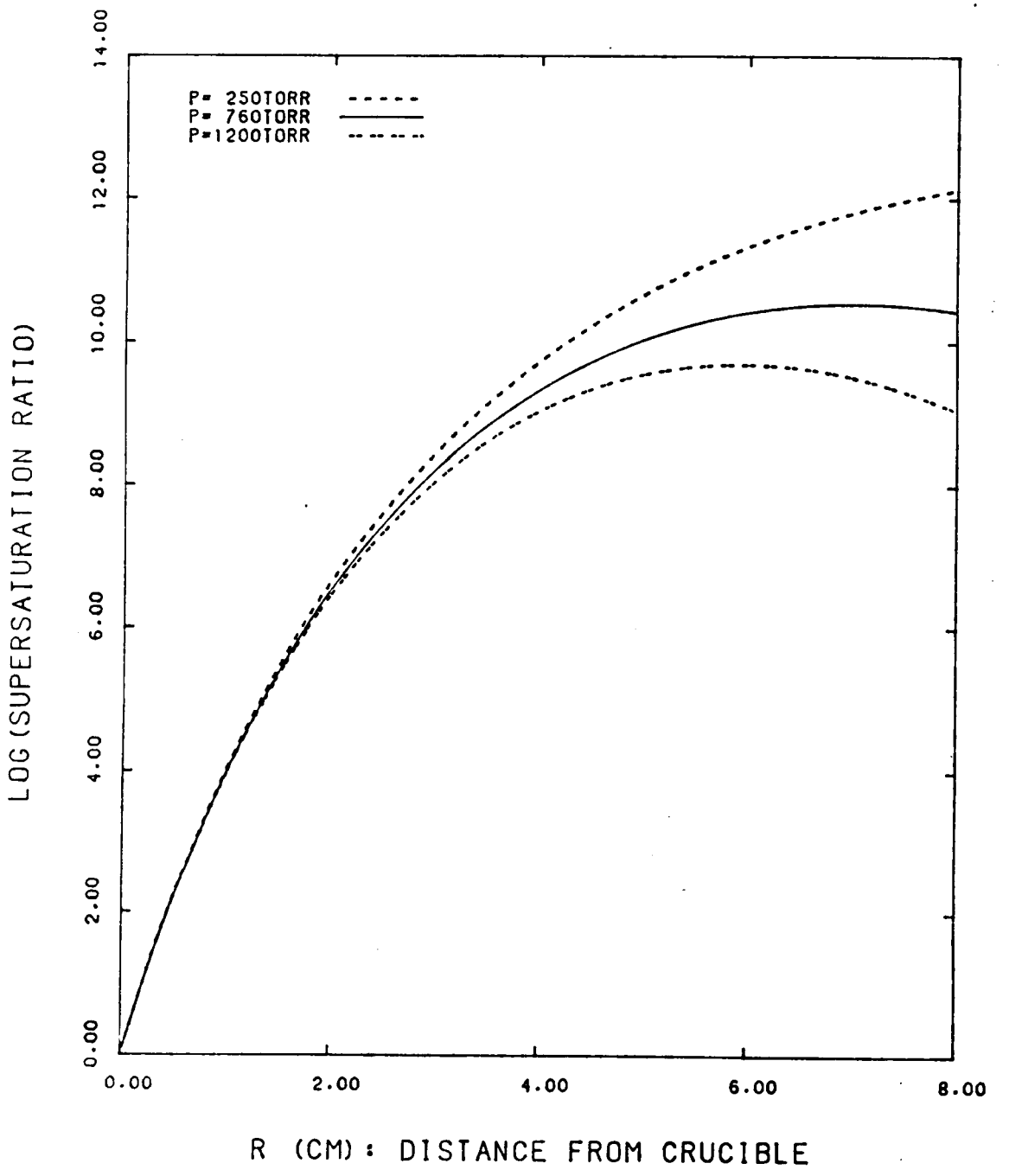

Figure 4-10: Effect of Total Pressure: t = 15 s

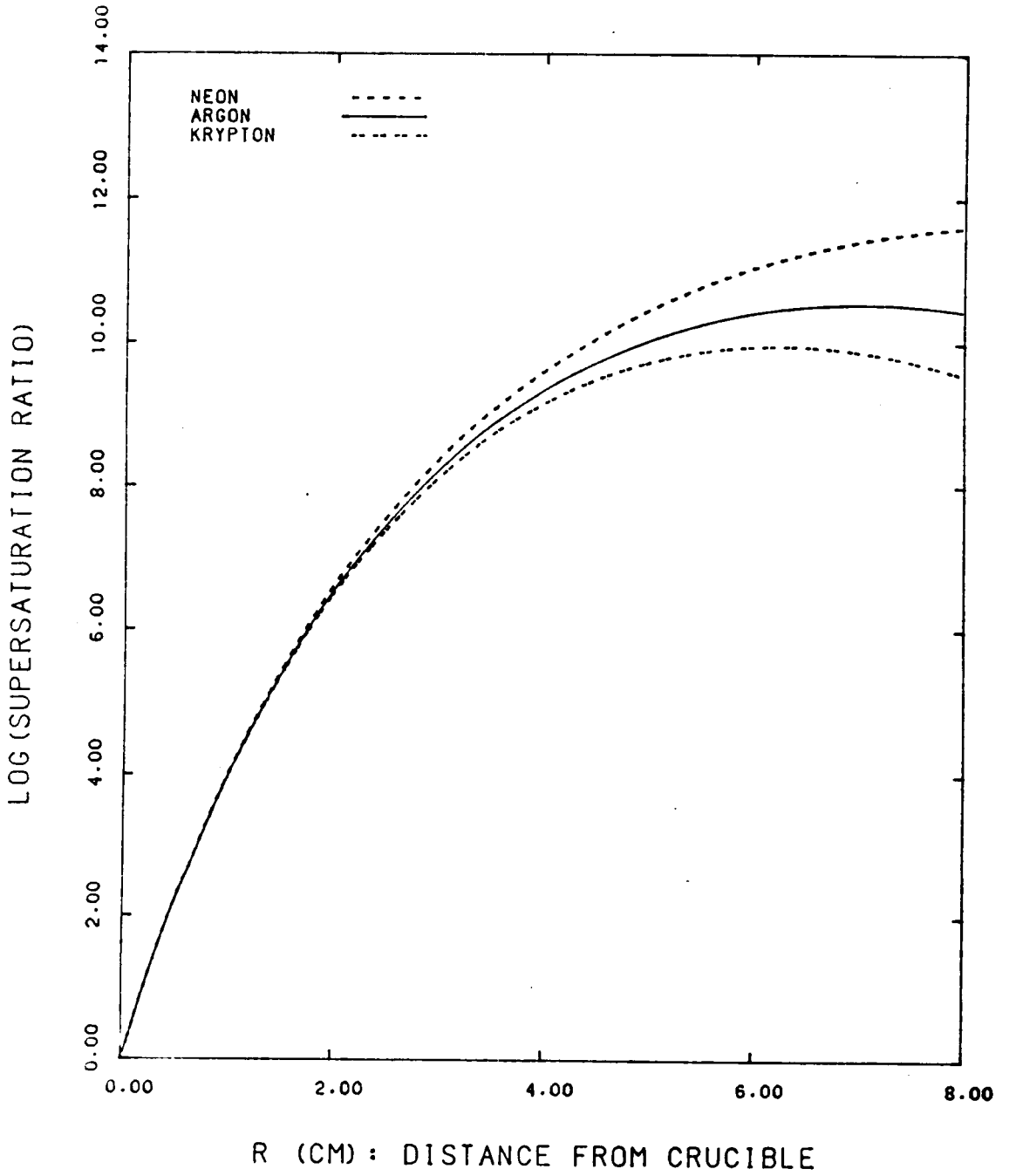

Figure 4-11: Effect of Ambient Gas: t = 15 s

4.5. Amount of Heat Required

In order to keep the temperature profile constant once steady state has been reached, the designer of the experimental apparatus needs to know how much heat needs to be added to the system at $R1$ and removed from the system at $R2$ so that $T1$ and $T2$ can be maintained at constant values. We know that

$$q_{in} = q_{acc} + q_{out} \tag{4.1}$$

where q_{in} is the heat added to the system at $R1$, q_{acc} is the heat accumulated in the experimental apparatus and q_{out} is the heat removed from the system at $R2$.

Crank [14, p.100] solves the problem of the hollow sphere for q_{acc} and q_{out}. The heat that accumulates between the two spheres is given by

$$q_{acc} = \frac{2}{3}\pi R1R2(R2-R1)\Delta H\left(\frac{R1}{R2}+0.5+\right.$$
$$\left.\frac{6}{\pi^2}\sum_{n=1}^{\infty}\frac{1}{n^2}\left(cos(n\pi)-\frac{R1}{R2}\right)exp\left(\frac{-\alpha(n\pi)^2 t}{(R2-R1)^2}\right)\right) \tag{4.2}$$

where ΔH is the change in enthalpy from $T1$ to $T2$ with units of cal/cm^3 and is calculated by

$$\Delta H = \int_{T2}^{T1} \rho C_p dT \tag{4.3}$$

The heat that needs to be removed from the system at $R2$ is given by

$$q_{out} = 2\pi R1R2(R2-R1)\Delta H(\frac{\alpha t}{(R2-R1)^2} - \frac{1}{6} - \frac{2}{\pi^2}\sum_{n=1}^{\infty}\frac{cos(n\pi)}{n^2}\times$$

$$exp(\frac{-\alpha(n\pi)^2 t}{(R2-R1)^2})) \qquad (4.4)$$

Then eqn.(4.2) and eqn.(4.4) can be substituted into eqn.(4.1) so that the total amount of heat needed to be added to the system can be calculated.

Figure 4-12 shows a plot of both heat rates vs. time for the Mg-Ar system. As can be seen, the input heat rate reaches a constant value of 0.290cal/sec after a period of approximately 5.5 minutes, and the heat rate out levels off at the same constant value of 0.290cal/sec after a period of approximately 10 minutes.

Another purpose of calculating the amount of heat added and removed is to give the designer a guideline when considering the type of material to be used for the outside wall. It is beyond the scope of this study to determine how thick the outside wall should be and what type of material should be used in order to maintain the derived surface temperature at $T2$.

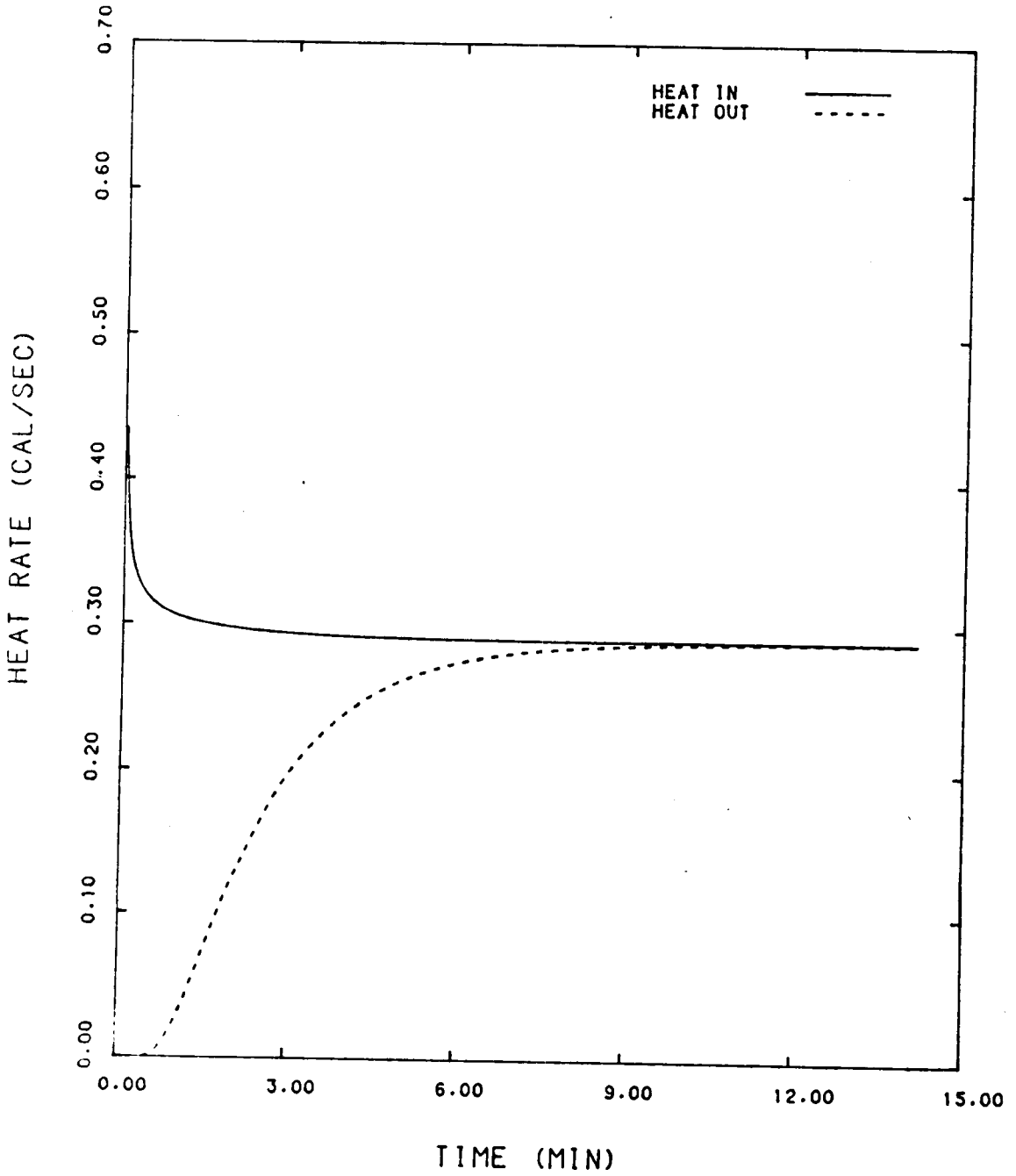

Figure 4-12: Heat Rate vs. Time

4.6. Temperature Profile: Flat Source

Consider the case in which the region $z > 0$ is continuously heated by a constant flux over a portion of its surface. More specifically, the heat supply is added at the rate q per unit time per unit area over a circular disk $x^2 + y^2 \leq R1$ when time $t \geq 0$ and $z = 0$. Carslaw and Jaeger [16, p.264] give a solution to this problem in terms of the temperature excess ($T_{ex} = T - T2$) along the direction (0,0,z) through and normal to the center of the circular disk heat source, and the equation is given by:

$$T_{ex} = \frac{2q\sqrt{\alpha t}}{k}\left(ierfc\left(\frac{z}{2\sqrt{\alpha t}}\right) - ierfc\left(\frac{\sqrt{z^2 + R1^2}}{2\sqrt{\alpha t}}\right)\right) \tag{4.5}$$

where k is the thermal conductivity, α is the thermal diffusivity and t is the time.

If the baseline conditions stated at the beginning of this chapter are used, then eqn.(4.5) can be solved for q when $z = 0$. The heat supply then remains constant for the entire temperature range. Also, since the temperature profile calculated by eqn.(4.5) is time dependent, a method is needed to determine the amount of time it will take before the baseline condition at the outer boundary is violated ($T2 > 293\ K$). For a first estimate, the amount of time it takes for the heat rate q_{in} calculated in the previous section is used; however, after 5.5 minutes, the temperature at the outside boundary ($R2 = 24$ cm) is greater than 293 K; therefore, a shorter time period is required.

If the system is allowed to run for a period greater than 113

seconds, then the boundary condition at $R2$ will be violated. Therefore, q is calculated for t = 113 s, and this value is then used to calculate the temperature profile.

Figure 4.13 shows the temperature profile for this system for several values of $R1$. A different value of q must be used for each temperature profile. Notice, that as $R1$ is increased, the temperature profile shifts to higher values and becomes less steep; therefore, the supersaturation ratio should decrease and the maximum value should move farther from the source as $R1$ is increased.

4.7. Comparison with Experimental Results

The only experimental data available at this time for comparison with these model predictions are those for the silver vapor-hydrogen gas system as reported by Donnelly [17]. Data generated from an adjusted hollow sphere model are compared with the experimental data obtained by Donnelly (see Table 4-3). This comparison is subject to the following assumptions. $T1$ is assigned the actual crucible temperature. $R1$ is assigned the actual crucible radius. $T2$ is adjusted to give the same approximate temperature, T_n, at the point of nucleation, r_n. $R2$ is chosen to correspond to the distance from the crucible to the thermocouple near the furnace. Finally, since no time interval is given with the experimental data, the data obtained from the hollow sphere model is calculated at steady state temperature and steady state partial pressure. The supersaturation ratios are then compared.

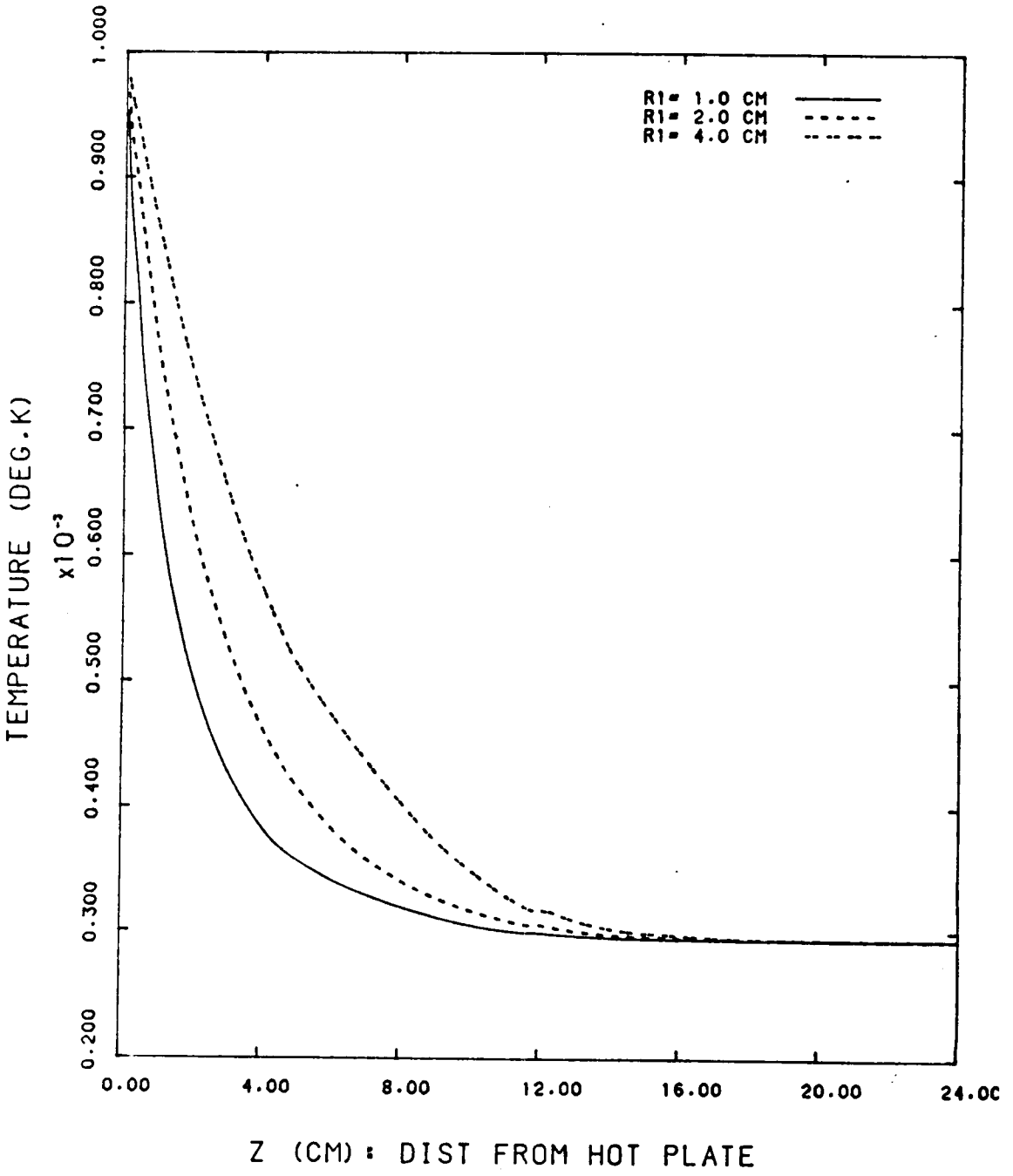

Figure 4-13: Temperature Profile: Flat Source

Table 4-3: Experimental vs. Model Comparison

The data are grouped in threes:
Experimental data by Donnelly [17]
Adjusted model prediction - constant α
Adjusted model prediction - variable α

Pressure = 250 torr

R1	R2	rn	T1	T2	Tn	Pp	S
(cm)	(cm)	(cm)	(K)	(K)	(K)	(torr)	----
0.95	7.64	4.77	1358	571	625	6.00E-04	1.00E11
0.95	7.00	4.80	1358	599	624.9	6.41E-04	1.07E11
0.95	7.00	4.80	1358	561	625.1	6.41E-04	1.05E11
0.95	7.64	4.77	1392	576	638	1.10E-03	6.30E10
0.95	7.00	4.80	1392	611	637.7	1.17E-03	6.69E10
0.95	7.00	4.80	1392	572	638.3	1.16E-03	6.36E10
0.95	7.64	4.77	1403	583	648	1.40E-03	3.40E10
0.95	7.00	4.80	1403	621	647.7	1.41E-03	3.59E10
0.95	7.00	4.80	1403	582	647.7	1.41E-03	3.58E10
0.95	7.64	4.13	1426	615	699	2.40E-03	1.40E09
0.95	7.00	4.10	1426	652	698.9	3.67E-03	2.16E09
0.95	7.00	4.10	1426	586	699.3	3.67E-03	2.10E09
0.95	7.64	4.77	1378	642	687	9.00E-04	1.20E09
0.95	7.00	4.80	1378	663	687.4	9.15E-04	1.20E09
0.95	7.00	4.80	1378	633	686.7	9.15E-04	1.26E09
0.95	7.64	4.77	1359	650	695	6.00E-04	4.90E08
0.95	7.00	4.80	1359	672	695.4	6.53E-04	4.88E08
0.95	7.00	4.80	1359	645	694.8	6.53E-04	5.12E08
0.95	7.64	4.77	1386	696	734	1.00E-03	6.20E07
0.95	7.00	4.80	1386	711	734.0	1.05E-03	6.34E07
0.95	7.00	4.80	1386	688	734.4	1.05E-03	6.19E07
0.95	7.64	5.09	1405	709	726	1.30E-03	1.30E08
0.95	7.00	5.10	1405	709	726.2	1.05E-03	1.04E08
0.95	7.00	5.10	1405	691	726.2	1.05E-03	1.04E08

As can be seen from Table 4-3, the model predictions compare favorably with the trend in the experimental data. Notice that the supersaturation ratios obtained by both the constant and variable thermal diffusivity temperature profiles have approximately the same distance to the outer boundary as that in the experiments. However, $T2$, the temperature required to match T_n, is greater for the constant α temperature profile. This is expected because in order for the two temperature profiles to be similar near the point of nucleation, $T2$ needs to be raised for the steady state temperature profile. This comparison is limited by the fact that because of the matched temperatures, the vapor pressure at the point of nucleation is identical for all three cases, and therefore, the only difference in the supersaturation ratio would be due to the difference in partial pressure.

These results do not prove that the hollow sphere model is totally accurate in calculating the supersaturation ratio since the model has been compared with only one system. However, the results do show that there is a strong possibility that the hollow sphere model can be used to predict a range of supersaturation ratios where nucleation is expected to occur. It must be noted that the question of which temperature profile is more accurate cannot be determined theoretically; therefore, the temperature profile must be carefully monitored in the upcoming experiments because it appears that the temperature profile has a significant effect on the supersaturation ratio.

Chapter 5
CONCLUSIONS

The hollow sphere model has been developed so that a range of supersaturation ratios can be determined. Also, the effects of each parameter on the supersaturation ratio has been examined. A comparison with available experimental data shows that the hollow sphere model may predict supersaturation ratios with some accuracy, but much more experimental data are needed before any final conclusions can be made.

It has been shown that the supersaturation ratio is significantly dependent on the temperature profile, which depends on the temperature at the inner and outer spheres and on the radii of the inner and outer spheres. It appears that the temperature at the outer sphere has the greatest impact on the supersaturation ratio: the lower the outside temperature, the faster the supersaturation ratio increases and the larger the maximum value of the supersaturation ratio. The radius of the inner sphere also has a large impact on the supersaturation ratio: the smaller the radius, the faster the supersaturation ratio increases and the larger the maximum value of the supersaturation ratio. But, the effect of the change in the inner radius is not as dramatic as that of the change in the temperature at the outer sphere.

During the actual experiment, however, the expected procedure is to increase the temperature at the inner sphere with each successive run.

Increasing this temperature will raise the maximum value of the supersaturation ratio, but once again, the change is not as dramatic as that of the change in the temperature at the outer sphere.

A comparison of the two temperature profiles, one with constant α and one with variable α, shows that the supersaturation ratio is depressed for variable α when the same conditions are used as for constant α. Therefore, it is much more likely for nucleation to occur if the constant α temperature profile were the more representative of the actual temperature profile achievable in the experimental apparatus.

Since the supersaturation ratio is dependent on the temperature of the system, it is imperative that the temperature profile in the experimental chamber be carefully monitored. Also, careful documentation of all future experiments must be recorded so that some of the guess work is deleted when comparing experimental data with model predictions. Most importantly, more experiments must be performed so that more experimental data can be examined, and the nucleation of refractory metal vapors can be better understood.

Chapter 6
BIBLIOGRAPHY

1. Nuth, J.A., and B. Donn, J. Chem. Phys. **77**, 2639 (1982).

2. Nuth, J.A., K.A. Donnelly, D. Donn, and L.U. Lilleleht, J. Chem. Phys. 85, 1116 (1986).

3. Becker, R., and W. Doring, Ann. Phys. **24**, 719 (1935).

4. Abraham, F.F., Homogeneous Nucleation Theory. Academic Press, Inc., 1974.

5. Adamson, A.W., Physical Chemistry of Surfaces. 4th ed. John Wiley & Sons, Inc., 1982.

6. Nuth, J.A., Ph.D. Dissertation, University of Maryland (1982).

7. Rasmussen, D.H., J. Cryst. Growth 56, 45 (1982).

8. Rasmussen, D.H., J. Cryst. Growth 56, 56 (1982).

9. Cahn, J.W., and J.E. Hilliard, J. Chem. Phys. **31**, 688 (1959).

10. Frurip, D.J., and S.H. Bauer, J. Phys. Chem. 81, 1001 (1977).

11. Freund, H.J., and S.H. Bauer, J. Phys. Chem. 81, 994 (1977).

12. Tolman, R.C., J. Chem. Phys. **17**, 3 (1949).

13. Nuth, J.A., M.W. Wiant and J.E. Allen, Jr., Astrophys. J. **293**, 463 (1985).

14. Crank, J., The Mathematics of Diffusion. 2nd ed. Oxford University Press, 1975.

15. Reid, R.C., J.M. Prausnitz and T.K. Sherwood, The Properties of Gases and Liquids. 3rd ed. McGraw-Hill Book Company, 1977.

16. Carslaw, J.W., and J.C. Jaeger, Conduction of Heat in Solids. 2nd ed. Oxford University Press, 1959.

17. Donnelly, K.A., Masters Thesis. University of Virginia (1985).

18. Handbook of Chemistry and Physics. 56th ed. The Chemical Rubber Co., 1975-1976.

19. Nesmayanov, A.N., Vapour Pressure of the Elements. Translated by J.I. Carasso. Academic Press, Inc., 1963.

20. Handbook of Chemistry and Physics. 53rd ed. The Chemical Rubber Co., 1972-1973.

21. Thermophysical Properties of Matter. Vol. 3. Purdue Research Foundation, 1970.

22. Thermophysical Properties of Matter. Vol. 6. Purdue Research Foundation, 1970.

Appendix A
General Properties

The following is a list of the general properties of the elements used in this study [18].

Argon

Molecular weight	39.948 g/g-mol
Heat capacity constants [15]	A_{Cp} = 4.969
	B_{Cp} = $-0.767*10^{-5}$
	C_{Cp} = $1.234*10^{-8}$
	D_{Cp} = 0.0

Hydrogen

Molecular weight	2.016 g/g-mol
Heat capacity constants [15]	A_{Cp} = 6.483
	B_{Cp} = $2.215X10^{-3}$
	C_{Cp} = $-3.298X10^{-6}$
	D_{Cp} = $1.826X10^{-9}$

Krypton

Molecular weight	83.800 g/g-mol

Magnesium

Molecular weight	24.312 g/g-mol
Melting point	922 K
Boiling point	1363 K
Antoine constants [19]	A_v = 8.589
	B_v = -7527

Neon

Molecular weight	20.183 g/g-mol

Silver

Molecular weight	107.868 g/g-mol
Boiling point	2485 K
Antoine constants [20]	A_v = 8.924812
	B_v = -14464.154

Appendix B
Thermal Diffusivity

The calculation of the steady state temperature profile developed in Section 2.1.2 requires knowledge of the temperature dependence of the thermal diffusivity. This dependence is determined by the properties of the inert gas in the chamber since the concentration of the refractory vapors is very low and is not expected to affect the thermal diffusivity. The thermal diffusivity is defined by the following equation

$$\alpha = \frac{k}{\rho C_p} \qquad (B.1)$$

where α is the thermal diffusivity with units cm^2/s, k is the thermal conductivity with units cal/(cm-s-K), ρ is the molar density with units g-mol/cm^3 and C_p is the heat capacity with units cal/(g-mol-K).

The molar density is calculated using the ideal gas law:

$$\rho = \frac{P}{RT} \qquad (B.2)$$

where T is in degrees Kelvin, P has units of torr and R is the gas constant with units of cm^3-torr/(g-mol-K).

The heat capacity is assumed to depend on temperature according to the relationship:

$$C_p = A_{Cp} + B_{Cp}T + C_{Cp}T^2 + D_{Cp}T^3 \qquad (B.3)$$

where A_{Cp}, B_{Cp}, C_{Cp} and D_{Cp} are constants listed in Appendix A.

Argon

A linear relationship is often used for the temperature dependence of the thermal conductivity:

$$k = k_o + aT \qquad (B.4)$$

A plot of k vs. T for argon can be divided into three linear sections [21]. The first section is for temperatures less than 350 K and is represented by:

$$k_{Ar} = 3.5114967\times10^{-6} + 1.2992085\times10^{-7}T \qquad (B.5)$$

The second section is for temperatures between 350 K and 600 K and follows the relationship:

$$k_{Ar} = 1.5159706\times10^{-5} + 9.5151565\times10^{-8}T \qquad (B.6)$$

For temperatures above 600 K, the following relationship is used:

$$k_{Ar} = 2.7637119\times10^{-5} + 7.4903601\times10^{-8}T \qquad (B.7)$$

Next, the thermal diffusivity can be calculated as a function of temperature and pressure. If we plot α vs. T on log-log paper over the entire temperature range, we get the following approximate relationship:

$$\alpha_{Ar} = 8.32\times10^{-3}\frac{T^{1.73}}{P} \qquad (B.8)$$

This equation is used to determine the effect of the thermal diffusivity on the temperature profile as calculated in Section 2.1.2.

Krypton

The specific heat of krypton is assumed to be constant over the temperature range of 10 K < T < 6200 K. Therefore C_p is given by the following equation:

$$C_{p_{Kr}} = \frac{5R}{2M_{Kr}} = 0.059284 \qquad (B.9)$$

where R is the gas constant in units of cal/g-mol-K and M_{Kr} is the molecular weight of krypton [22].

The thermal conductivity for krypton is given by the following equation:

$$10^5 k_{Kr} = 9.06926\times10^{-3} + 8.33613\times10^{-3}T - 2.87117\times10^{-6}T^2 \qquad (B.10)$$

where k is in cal/cm-s-K and T is in degrees Kelvin [21].

If α vs. T is plotted on log-log paper, the following approximate relationship is given for the thermal diffusivity:

$$\alpha_{Kr} = 4.0236\times10^{-3}\frac{T^{1.75}}{P} \qquad (B.11)$$

Neon

The specific heat of neon is assumed to be constant over the temperature range of 10 $K < T <$ 8000 K. Therefore, C_p is given by the following equation:

$$C_{p_{Ne}} = \frac{5R}{2M_{Ne}} = 0.24615 \qquad (B.12)$$

where R is the gas constant in units of cal/g-mol-K and M_{Ne} is the molecular weight of neon [22].

The thermal conductivity for neon is given by the following equation:

$$10^5 k_{Ne} = 0.49159 + 5.47196\times10^{-2}T - 7.1979\times10^{-5}T^2 + 5.06172\times10^{-8}T^3 \qquad (B.13)$$

where k is in cal/cm-s-K and T is in degrees Kelvin [21].

If α vs. T is plotted on log-log paper, the following approximate relationship is given for the thermal diffusivity:

$$\alpha_{Ne} = 1.3298\times10^{-2}\frac{T^{1.8}}{P} \qquad (B.14)$$

If eqn.(B.8), eqn.(B.11) and eqn.(B.14) are compared, the temperature dependence is approximately the same for each element; therefore, the inert gas should not have a significant effect the temperature profile developed in Section 2.1.2.

Appendix C
Molecular Diffusion Coefficient

The general equation used to calculate the diffusion coefficient for species A in a binary gas mixture is given by [15]:

$$D_{A-B} = 1.858\times10^{-3}\frac{T^{1.5}(M_A+M_B)^{0.5}}{P\sigma^2{}_{A-B}\Omega_D(M_AM_B)^{0.5}} \qquad (C.1)$$

where:

$D_{A\text{-}B}$ = diffusion coefficient for components A and B, cm^2/s
T = temperature, K
P = total pressure, atm
σ = characteristic length, angstroms
Ω_D = diffusion collision integral, dimensionless
M_A = molecular weight of component A, g/g-mole
M_B = molecular weight of component B, g/g-mole

with:

$$\Omega_D = \frac{A}{(T^*)^B}+\frac{C}{\exp(DT^*)}+\frac{E}{\exp(FT^*)}+\frac{G}{\exp(HT^*)} \qquad (C.2)$$

where

A = 1.06036 $\quad$ E = 1.03587
B = 0.15610 $\quad$ F = 1.52996

C = 0.19300 G = 1.76474
D = 0.47635 H = 3.89411

$$T^* = \frac{kT}{\epsilon_{A-B}}$$

The Lennard-Jones parameters are given by:

$$\sigma_{A-B} = \frac{\sigma_A+\sigma_B}{2} \qquad (C.3)$$

$$\epsilon_{A-B} = \sqrt{\epsilon_A \epsilon_B} \qquad (C.4)$$

C.1. Magnesium-Argon System

The values used to calculate the diffusion coefficient for the magnesium-argon system were

σ_{Mg} = 2.72 angstroms
σ_{Ar} = 3.542 angstroms

$$\frac{\epsilon_{Mg}}{k} = 1.15T_b = 1.15(1363) = 1567.6K$$
$$\frac{\epsilon_{Ar}}{k} = 93.3K$$

M_{Mg} = 24.305g/g-mole
M_{Ar} = 39.948g/g-mole

By using eqn.(C.3) and eqn.(C.4)

$$\sigma_{\text{Mg-Ar}} = 3.131 \text{ angstroms}$$

$$\frac{\epsilon_{Mg-Ar}}{k} = 382.44K$$

Therefore, eqn.(C.1) becomes:

$$D_{Mg-Ar} = 4.877\times10^{-5}\frac{T^{1.5}}{P\Omega_D} \qquad (C.5)$$

C.2. Magnesium-Krypton

Following the same procedure as in Appendix C.1, eqn.(C.3) and eqn.(C.4) become:

$$\sigma_{\text{Mg-Kr}} = 3.1875 \text{ angstroms}$$

$$\frac{\epsilon_{Mg-Kr}}{k} = 529.5693K$$

Therefore, eqn.(C.1) becomes:

$$D_{Mg-Kr} = 4.2134\times10^{-5}\frac{T^{1.5}}{P\Omega_D} \qquad (C.6)$$

C.3. Magnesium-Neon

Following the same procedure as in Appendix C.1, eqn.(C.3) and eqn.(C.4) become:

$$\sigma_{\text{Mg-Ne}} = 2.77 \text{ angstroms}$$

$$\frac{\epsilon_{Mg-Ne}}{k} = 226.7538K$$

Therefore, eqn.(C.1) becomes:

$$D_{Mg-Ne} = 7.29268\times10^{-5}\frac{T^{1.5}}{P\Omega_D} \qquad (C.7)$$

C.4. Silver-Hydrogen

Following the same procedure as in Appendix C.1, eqn.(C.3) and eqn.(C.4) become:

$$\sigma_{\text{Ag-H}_2} = 2.8545 \text{ angstroms}$$

$$\frac{\epsilon_{Ag-H_2}}{k} = 413.05K$$

Therefore, eqn.(C.1) becomes:

$$D_{Ag-H_2} = 7.29268\times10^{-5}\frac{T^{1.5}}{P\Omega_D} \qquad (C.8)$$

Appendix D
Computer Program

```
PROGRAM SUP_SAT_P  (input, output);

(*********************************************************************)
(*                                                                   *)
(*  This program calculates the supersaturation ratio for a gaseous *)
(*  Mg & Ar system using an equation from Crank(p.100) for a hollow *)
(*  sphere with an inside radius of R1 and an outside radius of R2. *)
(*  The equation is used to calculate the temperature profile and   *)
(*  the partial pressure profile.                                    *)
(*                                                                   *)
(*********************************************************************)

const   pi = 3.1415927;       gasR = 82.06;    (* cm^3-atm/mol-deg.K*)
         A = 1.06036;         B = 0.15610;
         E = 0.19300;         F = 0.47635;
         G = 1.03587;         H = 1.52996;
         J = 1.76474;         L = 3.89411;

var     i: integer;
        ss,time,time1,r,R1,R2,R3: real;
        sine,expo,T,T1,T2,P,Tex,Tx,Pp,Pv,Ssat,log: real;
        ssP,ad,D,ad_summ,summ,P1,omega,ek,T3: real;
        response: char;

procedure introduction(var P,T1,T2,time1,R1,R2,R3: real);

begin
writeln('Supersaturation Ratio for Mg & Ar');
writeln;writeln;
write('Select the ambient gas pressure(mmHg): ');
readln(P); writeln;
write('Select the hot temperature surface(deg. K): ');
readln(T1); writeln;
write('Select the cold temperature surface(deg. K): ');
readln(T2); writeln;
```

```
write('Select the time step(sec): ');
readln(time1); writeln;
write('Select the inner radius(cm): ');
readln(R1); writeln;
write('Select the outer radius(cm): ');
readln(R2); writeln;
write('Select the step size for the radius(cm): ');
readln(R3);writeln;writeln;writeln;
end;

procedure heading;

begin
writeln('SUPERSATURATION RATIO FOR Mg & Ar');
writeln('-------------------------------');
writeln;writeln;
writeln('Gas Hemisphere Radius = ', R2:19:1,' cm');
writeln('Hot Surface Radius    = ', R1:19:1,' cm');
writeln('Ambient Gas Pressure  = ', P:19:1,' mmHg');
writeln('Temperature: hot surface  = ',T1:15:1,' deg. K');
writeln('             cold surface = ',T2:15:1,' deg. K');
writeln;writeln;
writeln('Temperature excess above the cold surface: Tex(deg. K)');
writeln('Distance from hot surface: r(cm)');
writeln;writeln;
writeln('t':3,'r':6,'T':10,'Pp':11,'Pv':11,'Ssat':12,'log(Ssat)':13);
writeln('(sec)':5,'(cm)':5,'(deg.K)':11,'(mmHg)':10,'(mmHg)':11);
write('-------------------------------------------------------------');
writeln('---------');
writeln;
end;

procedure diff_coef(T,P:real; var D:real);

(*********************************************************************)
(*                                                                   *)
(*     The diffusion coefficient for the Mg-Ar system is             *)
(*     calculated in Appendix C. Also, any of the other              *)
(*     diffusion coefficients calculated in Appendix C               *)
(*     may be substituted in this procedure.                         *)
(*                                                                   *)
(*********************************************************************)

begin
```

```
    ek:= 382.44;      (* deg.K *)
    T3:= T/ek;
    omega:= A/exp(B*ln(T3)) + E/exp(F*T3) + G/exp(H*T3) + J/exp(L*T3);
    D:= 4.877E-05*exp(1.5*ln(T))*760/(P*omega)     (* cm^2/sec *)
end;

(*****************************************************************)
(*                                                               *)
(*     The partial pressure profile is calculated using an       *)
(*     equation from Crank (p.100).                              *)
(*                                                               *)
(*****************************************************************)

procedure ss_pres(r,R1,R2:real; var ssP:real);

begin
    ssP:= (R1/(r+R1))*((R2-(r+R1))/(R2-R1))          (* torr *)
end;

procedure pres(r,R1,R2,time,D:real; var ad_summ:real);

begin
    ad:= 0;
    i:= 0;
    REPEAT
       i:= i + 1;
       sine:= sin(i*pi*r/(R2-R1));
       expo:= exp(-D*sqr(i*pi)*time/sqr(R2-R1));
       summ:= (2/pi)*(R1/(r+R1))*(1/i)*sine*expo;
       ad:= ad + summ;
    UNTIL abs(summ) < 1.0E-20;
    ad_summ:= ad;
end;

procedure temp (r,R1,R2:real; var T:real);

(*****************************************************************)
(*                                                               *)
(* This steady state profile is calculated assuming constant     *)
(* thermal diffusivity. If eqn.(2.23) is substituted here then   *)
(* the temperature profile assuming variable thermal diffusivity *)
(* can be calculated.                                            *)
(*                                                               *)
(*****************************************************************)
```

```
begin
    ss:= (R1/(r+R1))*((R2-(r+R1))/(R2-R1));
    T:= (T1-T2)*ss + T2                          (* deg.K *)
end;

procedure vapor(T: real; var Pv: real);

(*****************************************************************)
(*                                                               *)
(*   The vapor pressure is calculated using the Antoine equation *)
(*   with the constants obtained from Nesmeyanov (pp. 175-179).  *)
(*                                                               *)
(*****************************************************************)

begin
    Pv:= exp(2.3025851*(8.589 - (7527/T)));     (* torr *)
end;

procedure ratio(Pp,Pv: real; var Ssat,log: real);

begin
    Ssat:= Pp/Pv;
    if Ssat <= 0 then
     log:= 0
    else
     log:= ln(Ssat)/2.3025851
end;

procedure iteration(R1,R2,R3,P1:real;var time,D,Pp,Pv,Ssat,log:real);

begin
    r:= r + R3;
    temp(r,R1,R2,T);
    Tex:= T-T2;
    diff_coef(T,P,D);
    ss_pres(r,R1,R2,ssP);
    pres(r,R1,R2,time,D,ad_summ);
    Pp:= P1*(ssP - ad_summ);
    if Pp < 1.0E-7 then
      Pp:= 0.0;
    vapor(T,Pv);
    ratio(Pp,Pv,Ssat,log);
    if time=15 then
    writeln(time:4:1,r:6:1,T:11:4,Pp:11,Pv:11,Ssat:11,log:11);
```

```
    end;

BEGIN   {main program}
 REPEAT
 introduction(P,T1,T2,time1,R1,R2,R3);
 heading;
 T:= T1;
 vapor(T,Pv);
 P1:= Pv;
 Pp:= Pv;
 time:= 0;
 r:=0;
 Tx:= T-T2;
 if time = 0 then
 begin
  While r <= (R2-R1-R3) do
  begin
   if r= 0 then
   begin
    vapor(T,Pv);
    Pp:= Pv;
    ratio(Pp,Pv,Ssat,log);
    writeln(time:4:1,r:6:1,T:11:4,Pp:11,Pv:11,Ssat:11,log:11);
   end;
   r:= r + R3;
   T:= T2;
   diff_coef(T,P,D);
   Pp:= 0;
   vapor(T,Pv);
   ratio(Pp,Pv,Ssat,log);
   Tx:= T - T2;
  end;
end;
REPEAT
writeln;
T:= T1;
Pp:= P1;
r:= 0;
time:=time + time1;
While r <= (R2-R1-R3) do
begin
    iteration(R1,R2,R3,P1,time,D,Pp,Pv,Ssat,log);
end;
UNTIL (time = 15);
```

```
 writeln;
 write('Do you want another iteration? '); readln(response);
 UNTIL response <> 'y'
END.
```

DISTRIBUTION LIST

Copy No.	
1	Dr. Joseph A. Nuth, III Code 691 NASA Goddard Space Flight Center Greenbelt, MD 20771
2 - 3*	NASA Scientific and Technical Information Facility P.O. Box 8757 Baltimore/Washington International Airport Baltimore, MD 21240
4	Dr. L. U. Lilleleht, CHE
5	Dr. E. L. Gaden, CHE, Chr.
6 - 7	Ms. E. H. Pancake, Clark Hall
8	SEAS Publications Files

* Reproducible copies

JO# 0751:vsh

UNIVERSITY OF VIRGINIA
School of Engineering and Applied Science

The University of Virginia's School of Engineering and Applied Science has an undergraduate enrollment of approximately 1,500 students with a graduate enrollment of approximately 560. There are 150 faculty members, a majority of whom conduct research in addition to teaching.

Research is a vital part of the educational program and interests parallel academic specialties. These range from the classical engineering disciplines of Chemical, Civil, Electrical, and Mechanical and Aerospace to newer, more specialized fields of Biomedical Engineering, Systems Engineering, Materials Science, Nuclear Engineering and Engineering Physics, Applied Mathematics and Computer Science. Within these disciplines there are well equipped laboratories for conducting highly specialized research. All departments offer the doctorate; Biomedical and Materials Science grant only graduate degrees. In addition, courses in the humanities are offered within the School.

The University of Virginia (which includes approximately 2,000 faculty and a total of full-time student enrollment of about 16,400), also offers professional degrees under the schools of Architecture, Law, Medicine, Nursing, Commerce, Business Administration, and Education. In addition, the College of Arts and Sciences houses departments of Mathematics, Physics, Chemistry and others relevant to the engineering research program. The School of Engineering and Applied Science is an integral part of this University community which provides opportunities for interdisciplinary work in pursuit of the basic goals of education, research, and public service.